GEOURBAN

SEVENTH FRAMEWORK PROGRAMME

CAPACITIES - ERA.Net RUS: Linking Russia to the ERA

Contract for: **Innovation Project**

D.4.2

EO Data Analysis Protocol (VHR)

Project acronym: **GEOURBAN**
Project full title: Exploitin**G** **E**arth **O**bservation in s**U**stainable u**RB**an pl**A**nning & ma**N**agement
Contract no.: ERA.Net-RUS-033
Date: 30/11/2012
Doc. Ref.: GEOURBAN_21_PT_KUZGUN
Book Captain: H.Şebnem DÜZGÜN
Contributors: Mahmut ÇAVUR
Serkan KEMEÇ
Arzu ERENER
Thomas ESCH
Issue: 1.0
Deliverable no.: D.4.2
Dissemination: CO

Document Status Sheet

Issue	Date	Author	Comments
0.0			
0.1			
0.2			
1.0			

TABLES

FIGURES

Table of Contents

1. Introduction

1.1. Purpose of the document

This document provides a protocol for the use of micro-scale EO-images to drive EO-based indicators to guide end-users. It contains information about general characteristics of Very High Resolution (VHR) images for micro-scale applications, literature research about existing algorithms which are used for various information extractions from VHR images and applications for GEOURBAN case study sites.

1.2. Definitions and acronyms

Acronyms

2DPCA	Two-Dimensional Component Analysis
DEM	Digital Elevation Model
DSM	Digital Surface Model
DTM	Digital Terrain Model
EO	Earth Observation
GA	Genetic Algorithm
GEOURBAN	ExploitinG Earth Observation in sUstainable uRBan plAnning & maNagement
GIS	Geographical Information Systems
Lidar	Light Detection and Ranging
LULC	Land Use Land Cover
MLC	Maximum Likelihood Classifier
MLP	Multi-Layer Perception
NN	Neural Network
PCA	Principal Component Analysis
RS	Remote Sensing
SVM	Support Vector Machine

1.3. Document references

- A.Thiele et al., (2007). “Building recognition from multi-aspect high resolution InSAR data in urban areas,” IEEE Trans. Geosci. RemoteSens. 45(11), 3583–3593.
- Aksoy, S., & Akcay, H. G. (2005). Multi-resolution segmentation and shape analysis for remote sensing image classification. *Recent Advances in Space Technologies, 2005. RAST 2005. Proceedings of 2nd International Conference on* (pp. 599 - 604).
- Aksoy, S., Koperski, K., & Tusk, C. (2009). Land Cover Classification with Multi-Sensor Fusion of Par tly Missing Data. *Photogrammetric Engineering & Remote Sensing*, *75*(5), 577-593.
- Amini, J., Lucas, C., Saradjian, M., Azizi, A. and Sadeghian, S., (2002). "Fuzzy Logic System for Road Identification Using IKONOS Images". Photogrammetric Record 17(99), pp. 493–503.
- Aytekin Ö., Erener A., Ulusoy İ. and Düzgün Ş., (2012). "Unsupervised building detection in complex urban environments from multispectral satellite imagery". International Journal of Remote Sensing, iFirst, 2011, 1–26. ISSN 0143-1161 print/ISSN 1366-5901, Vol. 33, No. 7, 10 April 2012, 2152–2177, http://dx.doi.org/10.1080/01431161.2011.606852
- Bacher, U. and Mayer, H., (2005). "Automatic Road Extraction From Multispectral High Resolution Satellite Images". In: Stilla U, Rottensteiner F, Hinz S (Eds) CMRT05. IAPRS, Vol. XXXVI, Part 3/W24 --- Vienna, Austria, August 29-30.
- Baltsavias E., Pateraki M., and Zhang L., (2001). "Radiometric and geometric evaluation of Ikonos geo images and their use for 3D building modelling". Proc. Joint ISPRS Workshop on High Resolution Mapping from Space, Hannover, Germany.
- Bayram, U., Can, G., Duzgun, S., Yalabik, N., (2011)." Evaluation of Textural Features for Multispectral Images ," SPIE Prague, Czech Republic
- Bayram, U., Can, G., Yuksel, B., Duzgun, S., Yalabik, N. (2011). "Unsupervised land use - land cover classification for multispectral images," IEEE 19th Conference Signal Processing and Communications Applications (SIU): .574-577, 20-22 April doi: 10.1109/SIU.2011.5929715, Antalya.

- Benediktsson A., Arnason K. and Peraresi M., (2001) "The use of morphological profiles in classification of data from urban areas". In IEEE/ISPRS Joint Workshop on Remote Sensing and Data Fusion over Urban Areas, Print ISBN: 0-7803-7059-7, pp. 30–34.
- Benediktsson J.A., I. Kanellopoulos, (1999). IEEE Trans. Geosci. Remote Sens. 37(3), 1367.
- Benz, U., Hofmann, P., Willhauck, G., Lingenfelder, I., & Heynen, M. (2004). "Multi-resolution, objectoriented fuzzy analysis of remote sensing data for GIS-ready information". ISPRS Journal of Photogrammetry and Remote Rensing, 58, 239–258.
- Bicego, G et al (2003). "Dimensions of the Emerging Orphan Crisis in Sub Saharan Africa". Social Science and Medicine , 56, 1235-1247.
- Blaschke, T. (2010). "Object based image analysis for remote sensing". ISPRS Journal of Photogrammetry and Remote Sensing,65(1),2–16.
- Brodley, C. E., and Utgoff, P. E., (1995). "Multivariate decision trees". Machine L earning, 19, 45–77.
- Colesanti, C., A. Ferretti, F. Novali, C. Prati, F. Rocca, (2003). "SAR monitoring of progressive and seasonal ground deformation using the permanent scatterers technique, Geoscience and Remote Sensing". IEEE Transactions on Vol 41, 1685-1701.DeFries, R. S., Hansen, M., Townshend, J. R. G., and Sohlberg, R., 1998, Global land cover classi. cations at 8km spatial resolution: the use of training data derived from Landsat imagery in decision tree classi. ers. International Journal of Remote Sensing, 19, 3141–3168.
- Coppin, J., Jonckheere, I., Nackaerts, K. & Muys, B. (2004). Digital change detection methods in ecosystem monitoring: A review. *International Journal of Remote Sensing*, *10*, 1565-1596.
- Coppin, P.R. & Bauer, M.E. (1996). Digital Change Detection in Forest Ecosystems
- Dell'Acqua, F. & Gamba, P. (2003). "Texture-based characterization of urban environments on satellite SAR images". IEEE Transactions on Geoscience and Remote Sensing. Vol 41, No. 1, pp. 153-159.

- Dell'Acqua, F. (2009). "The role of SAR sensors". In Global mapping of human settlements: Experiences, Data Sets, and Prospects. Edited by P. Gamba and M. Herold. Taylor and Francis, Boca Raton. Pp. 209-319.
- Düzgün, H.S. and Demirel N., (2011). "Remote Sensing of the Mine Environment", pp. 35-82.
- Esch T, Taubenböck H, Roth A, Heldens W, Felbier A, Thiel M, Schmidt M, Müller A & Dech S (2012). "TanDEM-X mission: New perspectives for the inventory and monitoring of global settlement patterns". In: Journal of Selected Topics in Applied Earth Observation and Remote Sensing. Vol 6. p.22.
- Esch T, Thiel M, Schenk A, Roth A, Müller A & Dech S (2010). "Delineating of urban footprints from TerraSAR-X data by analyzing speckle characteristics and intensity information". IEE Transactions on Geoscience and Remote Sensing. Vol 48. No. 2. 905-916
- Esch T., V. Himmler, G. Schorcht, M. Thiel, C. Conrad, T. Wehrmann, F. Bachofer, M. Schmidt and S. Dech, (2009). "Large-area Assessment of Impervious Surface based on Integrated Analysis of Single-date Landsat-7 Images and Geospatial Vector Data". Remote Sensing of Environment, Vol. 113, issue 8, pp. 1678 - 1690.
- Esch, T., Schenk, A., Ullmann, T., Thiel, M., Roth, A. and S. Dech, (2011). "Characterization of Land Cover Types in TerraSAR-X Images by Combined Analysis of Speckle Statistics and Intensity Information". IEEE Trans. Geosci. Remote Sens., IEEE Xplore 10.1109/TGRS.2010.2091644.
- Esch, T., Thiel, M. Schenk, A. Roth, A. Müller, A. and S. Dech, (2010). "Delineation of Urban Footprints from TerraSAR-X Data by Analyzing Speckle Characteristics and Intensity Information", IEEE Transactions on Geoscience and Remote Sensing – Special Issue on TerraSAR-X, 2010, 905-916. DOI: 10.1109/TGRS.2009.2037144.
- Ferretti, A., C. Prati and F. Rocca, (2000). "Nonlinear subsidence rate estimation using permanent scatterers in differential SAR Interferometry", IEEE Trans. Geoscience Remote Sensing 38(5), 2202-2212.
- Ferretti, A., C. Prati, and F. Rocca, (2001). "Permanent scatterers in SAR Interferometry", IEEE Trans. Geosci. Remote Sensing, 39(1), 8-20.Friedl, M. A., and

Brodley, C. E., (1997). Decision tree classification of land cover from remotely sensed data. Remote Sensing of Environment, 61, 399–409.

- Gamba et al., (2006) “Improving building footprints in InSAR data by comparison with LIDAR DSM,” Photogramm. Eng. Remote Sens. 72(1), 63–70.
- Gereke M., Straub B.-M.and Koch A., (2001). "Automatic Detection of Buildings and Trees from Aerial Imagery, Using Different Levels of Abstraction". Publications of the German Society for Photogrammetry and Remote Sensing, vol X.E. Seyfert, Ed., pp. 273-280.
- Grey, W. & Luckman, A. (2003). "Mapping urban extent using satellite radar interferometry, Photogramm". Eng. Remote Sensing, 69(9): 957-961.
- Guo D., Weeks A., Klee H., (2004). "Segmentations Of Road Area in High Resolution Images". IGARSS 2004 : Science for society: exploring and managing a changing planet 2004 IEEE International Geoscience and Remote Sensing Symposium (proceedings) (Anchorage, Alaska).
- Haverkamp D., (2004). "Automatic building extraction from IKONOS imagery". In Proceedings of ASPRS 2004 Conference, Denver, CO.
- Herman M. and Kanade T., (1986). "Incremental reconstruction of 3D scenes from multiple, complex images". Artificial Intell., vol. 30, pp. 289-341, 1986.
- Heynen, M. (2004). "Multi-resolution, object-oriented fuzzy analysis of remote sensing data for GIS-ready information". ISPRS Journal of Photogrammetry and Remote Sensing, 58, 239-258.
- Huang, C., Davis, L.S. and Townshend, J.R.G (2002). "An assessment of support vector machines for land cover classification, International Journal of Remote Sensing" 23:4, 725-749.
- Huertas A. and Nevatia R., (1988). "Detecting Buildings in Aerial Images, Computer Vision, Graphics, and Image Processing" 41, pp. 131-152.
- Inglada, J. and Christophe, E., (2007). "Automatic recognition of man-made objects in high resolution optical RS images by SVM classification of geometric image features". ISPRS Journal of Photogrammetry and Remote Sensing. ISPRS Journal of Photogrammetry and Remote Sensing Volume 62, Issue 3, Pages 236-248.

- Irving R. and McKeown D.M., (1989). "Methods for Exploiting the Relationship between Buildings and Their Shadows in Aerial Imagery"; IEEE Transactions on Systems, Man, and Cybernetics, Vol.19, No.6, pp.1564-1575.
- Jensen, J.R., Cowen, D., Narumalani, S. & Hall, J. (1997). *Principles of change detection using digital remote sensor data.* Cambridge University Press. Cambridge, United Kingdom. 1997.
- Katartzis A. and Sahli H., (2008). "A Stochastic Framework for the Identification of Building Rooftops Using a Single Remote Sensing Image", IEEE Transactions on Geoscience and Remote Sensing, Vol.46, No.1, pp.259-271
- Kim Z.W., and Nevatia R., (1999). "Uncertain Reasoning and Learning for Feature Grouping, Computer Vision and Image Understanding", Vol.76, No3, pp.278-288
- Klang D., (1998). "Automatic Detection of Changes in Road Databases Using Satellite Imagery". In: International Archives of Photogrammetry and Remote Sensing, vol. 32 no.4/1, pp. 293– 298.
- Krishnamachari S. and Chellappa R., (1996). "Delineating Buildings by Grouping Lines with MRFs. Image Processing", on IEEE Trans. vol. 5, pp. 164-168.
- Laptev I., H. Mayer, T. Lindeberg, W. Eckstein, C. Steger, A. Baumgartner, (2000). Vis. Appl. 12, 23
- Li, Z., Zhu, Q. and Gold, C. (2005), Digital terrain modeling: principles and methodology, CRC Press. Boca Raton.
- Lin C. and Nevatia R., (1998). "Building detection and description from a single intensity image". Computer Vision and Image Understranding, vol. 72, pp. 102-121.
- Lin C. and Nevatia R., (1998). "Building Detection and Description from a Single Intensity Image" Computer Vision and Image Understanding, Vol.72, No.2, pp.101- 121
- Lippman, R. P., (1987). "An introduction to computing with neural nets". IEEE ASSP Magazine, 4, 2–22.
- Lizarazo I. and Elsner P., (2009). "Fuzzy segmentation for object-based image classification". International Journal of Remote Sensing, Vol. 30, No. 6, 20 pp. 1643–1649.

- Lu, D., Mausel, P., Brondizio, E. and Moran, E., (2004). “Change detection techniques”. International Journal of Remote Sensing, 25, 2365 - 2407.
- Lunetta, R.S. & Elvidge, C.D. (1998). *Remote sensing change detection; environmental monitoring methods and applications.* Ann Arbor Press. Chelsea, MI, UnitedStates.
- Mas,J.F. (1999). "Monitoring land cover changes: A comparison of change detection techniques". International Journal of RemoteSensing, 20(1),139–152.
- Matikainen,J. Hyyppä, and E.Engdahl, (2006). “Mapping built-up areas from multitemporal interferometric SAR images: a segment-based approach,” Photogramm.Eng.RemoteSens. 72(6), 701–714.
- Matsuyama T. and Hwang V.S.S.,(1990). "SIGMA: A Knowledge Based Aerial Image Understanding System". New York: Plenum.
- Mausel P.W., W.J. Kramber, J.K. Lee, (1990). Photogramm. Eng. Remote Sens. 56, 55.
- Meir Barzohar, David B. Cooper, (1996). "Automatic Finding of Main Roads in Aerial Images by Using Geometric-Stochastic Models and Estimation". IEEE Trans. Pattern Anal. Mach. Intell. 18(7): 707-721.
- Mena J.B., J.A. Malpica, (2005). Pattern Recognit. Lett. 26, 1201.
- Millward, A.A., Piwowar, J.M. & Howarth, P.J., (2005). Time-series analysis of medium-resolution, multisensor satellite data for identifying landscape change. *Photogrammetric Engineering and Remote Sensing.*
- Muller J.P., Ourzik C., Kim T., and Dowman I.J., (1997). "Assessment of the effects of resolution on automated DEM and building extraction". Automatic Extraction of Man-Made Objects from Aerial and Space Images (II), pp. 245–256, Birkhauser Verlag, Basel, Switzerland.
- Pal C., Swayne D., and Frey B., (2001). "The Automated Extraction of Environmentally Relevant Features from Digital Imagery Using Bayesian Multi-Resolution Analysis, Advances in Environmental Research", 5, pp.435-444.
- Paola, J. D., and Schowengerdt, R. A., (1995). "A review and analysis of back propagation neural networks for classification of remotely sensed multi-spectral imagery". International Journal of Remote Sensing, 16, 3033–3058.

- Pape, A.D., (2006). “Multiple Spatial Resolution Image Change Detection for Environmental Management Applications”. M.Sc. Thesis, University of Saskatchewan, Canada.
- Peng J. and Jin Y.Q., (2007). "An unbiased algorithm for detection of curvilinear structures in urban remote sensing images". International Journal of Remote Sensing, vol. 28, pp. 5377–5395, 10 December.
- Peng J. and Liu Y.C., (2005). "Model and Context-Driven Building Extraction in Dense Urban Aerial Images", International Journal of Remote Sensing, 26(7), pp.1289-1307.
- Perissin, D. and Feretti, A., (2007). "Urban-Target Recognition by Means of Repeated Spaceborne SAR Images". IEEE Transactions On Geoscience And Remote Sensing, Vol.45, No.12, 4043.
- Persson M., Sandvall M., and Duckett T., (2005). "Automatic Building Detection from Aerial Images for Mobile Robot Mapping Proceedings". 2005 IEEE International Symposium on Computational Intelligence in Robotics and Automation June 27-30, 2005, Espoo, Finland.
- Pesaresi M., (2000). "Texture analysis for urban pattern recognition using fine-resolution panchromatic satellite imagery". Geographical and Environmental Modelling, 4, pp. 43–63.
- Peteri R., and Ranchin T., (2003). "Multiresolution Snakes for Urban Road Extraction from Ikonos and Qickbird". In: EARSeL Symposium.
- Rufino, G.; Moccia, A.; Esposito, S. (1998). DEM generation by means of ERS tandem data. IEEE Transactions on Geoscience and Remote Sensing, 36(6), 1905-1912.
- Seetha, M. and Muralikrishna, I.V. (2008) “Artificial Neural Networks and Other Methods of Image Classification”. Journal of Theoretical and Applied Information Technology.
- Segl K. and Kaufmann H., (2001). "Detection of small objects from high-resolution panchromatic satellite imagery based on supervised image segmentation". IEEE Trans. Geosci. Remote Sensing, vol. 39, pp. 2080–2083.

- Shackelford, A., & Davis, C. H. (2003). “A combined fuzzy pixel-based and object-based approach for classification of high-resolution multispectral data over urban areas”. *Geoscience and Remote Sensing, IEEE Transactions on*, *41*(10), 2354-2364.
- Shan J. and Lee S., (2002). "Generalization of building polygons extracted from IKONOS imagery". Symposium on Geospatial Theory, Processing and Applications, Working Group IV/3, Ottowa.
- Singh, A., (1989). Digital Change detection Techniques Using Remotely Sensed Data. *International Journal of Remote Sensing*, *10*, 989-1003.
- Soergel, (2010). "Radar Remote Sensing of Urban Areas", p.277, Springer, Berlin.
- Sohn G., Dowman I.J., (2001). "Extraction of buildings from high resolution satellite data". In: Grün, A., Baltsavias, E.P., Henricsson, O. (Eds.), Automatic Extraction of Man-made Objects from Aerial and Space Images, vol. III. Balkema Publishers, Lisse, pp.345–356.
- Sohn H. G., Park C.H., Kim H.S., and Heo J., (2005). "3-D building extraction using IKONOS multispectral images". Geoscience and Remote Sensing Symposium, 2005. IGARSS '05. Proceedings. 2005 IEEE International, vol: 2, pp. 1432- 1434. ISBN: 0-7803-9050-4.
- Tarabalka, Y., Chanussot, J., & Benediktsson, J. A. (2010). Segmentation and classification of hyperspectral images using minimum spanning forest grown from automatically selected markers. *Systems, Man, and Cybernetics, Part B: Cybernetics, IEEE Transactions on*, *40*(5), 1267–1279. IEEE. doi:10.1109/TSMCB.2009.2037132
- Tatem A.J., Lewis H.G., Atkinson P.M. and Nixon M.S., (2001). "Super-resolution mapping of urban scenes from IKONOS imagery using a hopfield neural network". In Proceedings of IGARSS, 2001, Southampton, UK, pp. 3203–3205.
- Taubenböck H, Esch T, Wurm M, Roth A & Dech S (2010). "Object-based feature extraction using high spatial resolution satellite data of urban areas". In: Journal of Spatial Science, vol. 55, no. 1, pp. 117-133.
- Unsalan C. and Boyer K.L., (2005). "A System to Detect Houses and Residential Street Networks in Multispectral Satellite Images", Computer Vison and Image Understanding, 98, pp. 423-461.

- Venkateswar V. and Chellappa R., (1991). "A hierarchical approach to detection of buildings in aerial images". Tech. Rep. CAR-TR 567, Univ. of Maryland.
- Wang, P., Zhang, J.-xian, Jia, W.-jie, & Lin, Z.-jian. (2008). A study on decision tree classification method of land use/land cover -Taking tree counties in Hebei Province as an example. *2008 International Workshop on Earth Observation and Remote Sensing Applications*, 1-5. IEEE. doi:10.1109/EORSA.2008.4620331
- Wei L. and Prinet V., (2005). "Building Detection from High-resolution Satellite Image Using Probability Model". 0-7803-9050-4/05/$20.00 ©2005 IEEE.
- Wei Y., Zhao Z., and Song J., (2004). "Urban building extraction from high-resolution satellite panchromatic image using clustering and edge detection". Geoscience and Remote Sensing Symposium, IGARSS '04. Proceedings. 2004 IEEE International, vol. 3, pp.
- Wessel, B.; Gruber, A.; Gonzalez, J.H.; Bachmann, M.; Wendleder, A. (2008). TanDEM-X: DEM Calibration Concept. Proceedings of the 2008 IEEE International Geoscience and Remote Sensing Symposium, 111-114.
- Wilkinson G.G., (2005). "Results and implications of a study of fifteen years of satellite image classification experiments". IEEExplore
- with Remote Sensing Imagery. *Remote Sensing Reviews*, *13*, 207-234.
- Wurm M, Taubenböck H, Schardt M, Esch T & Dech S (2011). "Object-based image information fusion using multisensor earth observation data over urban areas". In: International Journal of Image and Data Fusion, 2(2), 121-147.
- Yang J., R.S. Wang, (2007). Int. J. Remote Sens. 28, 4653.
- Yuan, D., Elvidge, C.D. & Lunetta, R.S. (1998). Survey of Multispectral Methods for Landcover Change Analysis. *In* Lunetta, R.S. and C.D. Elsevier. 1998. *Remote Sensing Change Detection, Environmental Monitoring Methods and Applications.* Ann Arbour Press, Chelsea, Michigain
- Zhen G.Q., Shi, T.Z., Chun, L.Z. and Jin, Y.F., (2004). "Automatic building detection from high resolution images based on multiples features". In IEEE Commission II, ICWG II/IV.

2. Work Package Overview

WP4 includes the **micro-scale applications** in GEOURBAN case studies. Although previous research projects already addressed the use of very high spatial resolution (VHR) Earth Observation (EO) data in urban planning and management, **WP4** represents a unique attempt to collect and to analyze an integrated EO dataset suitable for the estimation of a subset of the EO-based indicators developed in WP3. The development of EO data analysis techniques is beyond the scope of GEOURBAN, therefore state of the art methods are used to derive specific products from raw EO datasets. VHR (e.g. Ikonos/Quickbird/WorldView/RapidEye/TerraSAR-X type) satellite data is used in the GEOURBAN case studies. The output of this WP4 is a set of products to be used as inputs for indicator evaluation and a report on the techniques used to derive these products from raw EO data.

3. Characteristics of Very High Resolution (VHR) Data

3.1. Introduction

The data obtained by using sensors without contacting the Earth surface is called remote sensing (RS) data. Acquiring data from the Earth by using RS relies on measuring and recording of electromagnetic radiation, which is also called irradiance, reflected from objects on the Earth's surface by the sensors. The sensors on satellite platforms have solid look angle and hence record spectral radiance of the Earth objects RS data can be classified based on various criteria. If the sensor's platform is of concern, the RS data can be obtained from either satellites or airplanes or ground platforms. The data obtained from satellites and airplanes are called satellite and aerial images, respectively. When the

energy source is considered, RS data can be obtained either from active or passive ways. When the sensor uses its own electromagnetic energy it is called active RS and radar sensors are of this type. When the sensor uses electromagnetic energy of the Sun then it are called passive RS and electro-optic sensors are of this type.

All RS data have four types of resolution namely, spatial, temporal, spectral and radiometric. Spatial resolution refers to the pixel size of the image which implies smallest object size that can be differentiated geometrically. Temporal resolution reflects the frequency of sensor's visit to the same location. Spectral resolution is the range of wavelength obtained by division of electromagnetic spectrum into wavelength intervals. Radiometric resolution defines the precision of the image's brightness values. The appraise RS data selection for extraction of urban planning requires consideration of the four resolution types. Very high resolution (VHR) RS data refers to spatial resolution of 5x5 m or less in GEOURBAN project. When the urban planning indicators are considered spatial resolution of 5x5 m or less is found to be appropriate for extracting related indicators. The temporal resolution is important for investigating the change in the indicators over a time period. Spectral resolution determines the extractability of indicators related with urban surface materials. VHR data with higher spectral resolution provides detection of object's material types as well as their geometries.

Most of the VHR data have spectral resolution of four spectral intervals which are also called bands, namely, Blue (B), Green (G), Red (R) and Near infrared (NIR). The VHR data can be obtained in stereo pair images from some of the satellites and stereo image processing products provide with 3D representation of the terrain and the objects on the terrain like built ups. The VHR data obtained from active RS can have various bands and be obtained in different polarizations. Properties of existing VHR data is given in Table 1 and
Table 2.

Before extracting any indicator form the VHR data based on image processing algorithms, images usually gone through three levels of pre-processing given in the following subsections

3.2. Pre-Processing of Image Data

It is applied in three levels. The first level (Level I) pre-processing involves **geometric and radiometric** correction. The second level (Level II) is **image enhancement** for better interpretation or information extraction. The third level is called **image transformation** which is carried out in order to extract specific characteristics like texture, vegetation, *etc*.

The level of pre-processing to be applied to VHR data depends on the accuracy level of the obtained data which are specified by the data providers and the information to be extracted from the data.

3.2.1. Level I-geometric and radiometric correction

This level pre-processing is mostly essential as the VHR data providers mainly do not provide geometrically corrected data. Each pixel of the image data corresponds to an area on the Earth's surface, which has certain positional information in the form of coordinates. The acquired image pixels may not be geometrically correct to indicate the actual locations of the objects due to geometric distortion occurred during image accusation. These geometric distortions may occur due to varying attitude, tilt, and velocity of the platform from which image is captured, type of the camera used for image acquisition and relief displacement of the ground. They have to be corrected before any information extraction.

Geometric correction of images is performed based on a two-step procedure. In the first step, mathematical transformation is applied to the raw image coordinates to obtain actual locations of the pixels. The procedure requires obtaining precise coordinates of some known features like road crossings; corners of the built ups etc. on the image as well as a digital terrain model (DTM) with resolution close to the spatial resolution of the VHR data.

The commonly used transformation functions are:

- Affine
- Bilinear
- Quadratic
- Bi-quadratic
- Cubic
- Bi-cubic

When an image is corrected for pixel locations, the new pixels of image represent the actual locations of pixels on the Earth. However, these pixels do not contain brightness values. Hence in the second step of geometric correction, the brightness values are resampled to be assigned to geometrically corrected pixels. The brightness values of the

corrected image can be obtained from brightness values of original image pixels by using the following sampling strategies:

- The nearest neighbor
- Bilinear interpolation
- Cubic convolution

In the **nearest neighbor** resampling method, the center coordinate of each pixel of the rectified image is found in the original image (raw image before rectification) and the nearest pixel center's brightness values in the original image is assigned to the rectified image pixel . In the **bilinear interpolation** resampling strategy, the four nearest neighbor pixel's brightness values are considered. The weighted average of the four neighboring brightness values is calculated and assigned to the pixel. In the **cubic convolution** method, the weighted average of the sixteen neighboring pixels based on the distance to the rectified pixel center is evaluated and assigned to the pixel of the rectified image.

The **radiometric correction** refers to compensation and removal of errors in the brightness values. These errors arise from sensors and atmospheric effects. Usually VHR data providers correct such errors before sending them to the customers.

Table 1. Properties of VHR data from various satellite sensors (Modified from Düzgün and Demirel 2011)

Sensor/Satellite	Operator/ Country	Launch and End Date	Sensor Type	Resolution			Revisit (days)
				Spectral Resolution (μm) or Polarimetry	Spatial (m)	Radiometic (bit)	
THEOS	GISTA/ Thailand	2008	PAN MS	0.45-0.90 0.45-0.52, 0.53-0.60, 0.62-0.69, 0.77-0.90	2 15	8 8	26 (14-5)
TOPSAT	BNSC-UK MoD/UK	2005	PAN MS	0.50-0.70 0.40-0.50, 0.50-0.60, 0.60-0.70	2.8 5.6	- -	4 (2-2.5)
WORLDVIEW-1	Digital Globe USA	2007	PAN	0.40-0.90 (S)	0.5	11	5
WORLDWIEW-2	Digital Globe USA	2009	PAN MS	0.45-0.80 (S) 0.40-0.45, 0.45-0.51, 0.51-0.58, 0.585-0.625, 0.63-0.69, 0.705-0.745, 0.77-0.895, 0.860-1.04 (S)	0.46 1.84	11 11	7 (1.1)
SPOT-5	CNES & Astrium/ France	2002	HRG-PAN	0.49-0.69 Super mode (S)	2.5-5	8	26 (1-4)
QUICKBIRD	Digital Globe USA	2001	PAN Multi	0.445-0.900 (S) VNIR: 0.45-0.52, 0.52-0.60, 0.63-0.69, 0.76-0.89 (S)	0.61-0.73 2.5-2.9	11 11	
TERRASAR-X	DLR&EADS Astium/ Germany	2007	Spotlight StripMap ScanSAR	X-Band λ: 0.03 m FRQ: 9.65 GHz Dual (HH+VH), Single (VV/HH) Single: VV/HH Dual: HH+VV/HH+HV/VV+HV Single: VV/HH	1 3 5 16	- - - -	15
PLEIADES-1&2	CNES/France	2010/2012	PAN MS	0.480-0.830 (S) 0.43-0.55, 0.49-0.61, 0.60-0.72, 0.75-0.94 (S)	0.5 (0.7) 2	12	26 (1)
RAZAKSAT-1	ATSB & TPM/Malasia	2009	PAN MS	0.51-0.73 0.45-0.52, 0.52-0.60, 0.63-0.69, 0.76-0.89	2.5 5	8 (10) 8 (10)	14

Table 2. Properties of VHR data from various satellite sensors (continued, Modified from Düzgün and Demirel)

Sensor/Satellite	Operator/ Country	Launch and End Date	Sensor Type	Resolution			Revisit (days)
				Spectral Resolution (μm) or Polarimetry	Spatial (m)	Radiometic (bit)	
RISAT-1	ISRO	2009	SAR	C-Band λ: 0.056 m FRQ: 5.35 GHz Single, Dual and Quad Pol.	3-50	-	12
DUBAISAT-1	EIAST/UAE	2009	PAN MS	0.42-0.89 (S CT) 0.42-0.51, 0.51-0.58, 0.60-0.72, 0.76-0.89 (S-CT)	2.5 5	8 8	5 (3) 5 (3)
EROS A1	ImageSat/ Israel	2000	PAN	0.5-0.9 (S)	1.9/0.9	10	1.8-4
EROS B1	ImageSat/ Israel	2006	PAN	0.5-0.9 (S)	0.7	10	1.8-4
FORMOSAT	NSPO/Taiwan	2004	PAN Multi	0.45-0.90 0.45-0.52, 0.52-0.60, 0.63-0.69, 0.76-0.90	2 8	8 8	1 1
GEOEYE-1	GeoEye/USA	2008	PAN Multi	0.45-0.80 0.45-0.51, 0.51-0.58, 0.655-0.69, 0.78-0.92			
IKONOS-2	GeoEye/USA Space Imaging	1999	PAN Multi	0.526-0.929 (S) 0.445-0.516, 0.516-0.595, 0.632-0.698, 0.757-0.853 (S)	0.82 3.2	11 11	
ALOS	JAXA/Japan	2006	PALSAR PRISM AVNIR/2	L-Band 1270 MHz, 23.6 cm Pan: 0.52-0.77 (Triplet) 0.42-0.50, 0.52-0.60, 0.61-0.69, 0.76-0.89	10-100 2.5 10	3/5 7 8	46 (2)
BEIJING-1	BLMIT/DMC/ China	2005	PAN Multi	0.5-0.8 0.52-0.62, 0.63-0.69, 0.76-0.9	4 32	8 10	14 5
CARTOSTAT-1 (IRS-P5)	ISRO/India	2005	PAN	0.5-0.85 (S)	2.5	10	126 (5)
CARTOSTAT-2	ISRO/India	2007	Mono Paint /Brush Multi-View	0.45-0.85	0.8	10	4-5
RAPIDEYE- 1/2/3/4/5	RapidEye/ Germany	2008	Multi	0.44-0.51, 0.52-0.59, 0.63-0.685, 0.69-0.73, 0.76-0.85	6.5	12	5.5

3.2.2. Level II-image enhancement

Image enhancement is not essential like **geometric and radiometric correction**. However, image enhancement may ease information extraction from the VHR data. Especially enhancements of spectral and spatial characteristics may improve visual image interpretation. The **spectral image enhancement** improves visual quality of the image by increasing the contrast and variability in brightness values between the pixels in the image data. Image histogram is one of the useful tools for assessing the radiometric quality of the images. Image filters are other useful tools for enhancing local image parameters. This type of enhancement works on the edge of the images because of the moving window approach which sharpens or smoothens the pixels.

3.2.3. Level III-image transformation

No matter the image is interpreted by digital image analysis or visual techniques, transforming images provides additional information. Image transformation methods can be divided into two categories:

• Transformations using single band of the image
• Transformations using several bands of the image

The most frequently applied image transformation to single band of the image is extraction of texture measures. Similar to spatial filtering, texture measures are local features inherent in the image. There are various transformations based on multiple bands on the image data. The most frequently used ones are:

• Transformation based on arithmetical operations,
• Vegetation indices,
• Principle Component Analysis (PCA), and
• Transformation into different color spaces.

3.3. Interpretation of VHR Data

The VHR data should be interpreted in order to obtain urban planning indicators. The interpretation can be performed either visual ways or using image analysis methods. Visual interpretation constitutes integrated analysis of the specific features related to the

Earth objects, namely, shape, size, tone, texture, pattern, shadow, association, and site (Düzgün and Demirel, 2011). The image analysis methods on the other hand uses sophisticated algorithms specifically developed for the following basic operations:

- Classification of the images
- Change analysis
- Digital surface and terrain modeling
- Feature extraction

Classification refers to grouping the object types existing in an image data. It is also called land use and land cover (LULC) classification, as the main aim is to categorize the landscape with its natural and man-made contents. Natural objects are forest, water, sand, *etc.* which are called land cover object classes. Man-made objects are urban, industrial; mine sites which are called land use object classes Figure 1. Land use is mainly governed by human activity and Land use and land cover are interrelated. Hence, any change in land cover can cause environmental changes, which, in turn, may have feedback effects on land cover and human driving forces that shape the direction and intensity of land-use.

The first step in any classification is to define the LULC class hierarchies, where for example CORINE (Coordination of Information on the Environment) or USGS land use/cover class hierarchies given in Table 3 and

Table 4, respectively can be used. The second step is to select a classification method. There are two different perspectives that can be used to the image for the classification procedure. These are pixel-based or object-based classification methods.

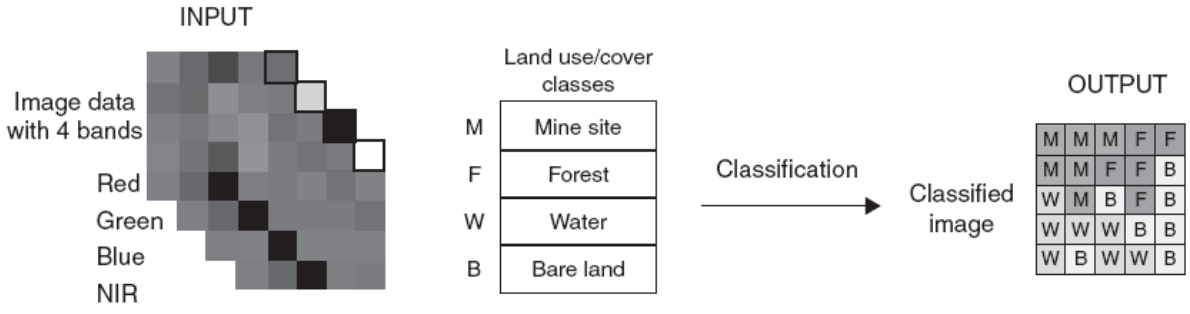

Figure 1. A typical image classification procedure (After Düzgün and Demirel, 2011).

Pixel-based classification assigns a class value to each pixel of the image. **Object-based classification** (also called object-oriented classification) relies on first segmenting the image into homogeneous regions and then assigning the classes to each segment (e.g. Blaschke, 2010; Taubenböck et al. 2010;Düzgün and Demirel, 2011).

Classification can be carried out based on **supervised classification algorithms** which comprise user interaction during classification procedure, where a data set called **training data** for each class is selected from the image by the analyst. Then the unclassified image pixels are settled on with the help of training data. **Unsupervised classification** on the other hand, does not require user interference into the classification procedure. It mainly establishes the relation between the spectral properties and classes which are inherent in the image and then by using the established relationship classification is performed. Both pixel-based and object-oriented perspectives and combinations of them can be used for supervised/unsupervised classification.

The unsupervised classification mainly relies on clustering algorithms which enables grouping the image pixels or segments based on spectral values. The only feedback from the user is the number of classes (clusters) to be formed through clustering algorithms. There are various types of clustering algorithms. Among the various clustering algorithms, **K-means clustering** is one of the most widely used methods in classification. The main steps of K-means clustering algorithms are as follows:

1. Determine k, which is number of classes.
2. Calculate an initial cluster centroid by obtaining a sample set which has k number of clusters with single element (data value of each element will be the initial centroid). It can be obtained by selecting arbitrary pixels or segments. Then assign each of the remaining sample set to the nearest centroid. Re-compute the centroid after each assignment. By this way, initial sets of k clusters are obtained.
3. Select each pixel or segment and compute its distance to each cluster centroid. Assign the pixel/object to the cluster with minimum distance and re-evaluate the cluster centroid after assignment.
4. Repeat step 3 until there is not any unclassified pixel/region is left.

Table 3. Land use/cover hierarchies of CORINE for RS.

Level I	Level II	Level III
1.Artificial surfaces	1.1. Urban fabric	1.1.1. Continuous urban fabric 1.1.2. Discontinuous urban fabric
	1.2. Industrial, commercial and transport units	1.2.1. Industrial or commercial units 1.2.2. Road and rail networks and associated land 1.2.3. Port areas 1.2.4. Airports
	1.3. Mine, dump and construction sites	1.3.1. Mineral extraction sites 1.3.2. Dump sites 1.3.3. Construction sites
	1.4. Artificial non-agricultural vegetated areas	1.4.1. Green urban areas 1.4.2. Sport and leisure facilities
2. Agricultural areas	2.1.Arable land	2.1.1. Non-irrigated arable land 2.1.2. Permanently irrigated land 2.1.3. Rice fields
	2.2. Permanent crops	2.2.1. Vineyards 2.2.2. Fruit trees and berry plantations 2.2.3. Olive groves
	2.3. Pastures	2.3.1. Pastures
	2.4. Heterogeneous agricultural areas	2.4.1. Annual crops associated with permanent crops 2.4.2. Complex cultivation 2.4.3. Land principally occupied by agriculture, with significant areas of natural vegetation 2.4.4. Agro-forestry areas
3. Forests and semi-natural areas	3.1. Forests	3.1.1. Broad-leaved forest 3.1.2. Coniferous forest 3.1.3. Mixed forest
	3.2. Shrub and/or herbaceous vegetation association	3.2.1. Natural grassland 3.2.2. Moors and heathland 3.2.3. Sclerophyllous vegetation 3.2.4. Transitional woodland shrub
	3.3. Open spaces with little or no vegetation	3.3.1. Beaches, dunes, and sand plains 3.3.2. Bare rock 3.3.3. Sparsely vegetated areas 3.3.4. Burnt areas 3.3.5. Glaciers and perpetual snow
4. Wetlands	4.1. Inland wetlands	4.1.1. Inland marshes 4.1.2.Peatbogs
	4.2. Coastal wetlands	4.2.1. Salt marshes 4.2.2. Salines 4.2.3. Intertidal flats
5. Water bodies	5.1. Inland waters	5.1. 1. Water courses 5.1.2. Water bodies
	5.2. Marine waters	5.2.1. Coastal lagoons 5.2.2. Estuaries 5.2.3. Sea and ocean

Table 4. Land use/cover hierarchies of USGS for RS.

Level I	Level II
1.Urban and built-up land	11 Residential 12 Commercial and service 13 Industrial 14 Transportation, communication and utilities 15 Industrial and commercial complexes 16 Mixed urban or built-up land 17 Other urban and built-up land
2. Agricultural land	21 Cropland and pasture 22 Orchards, groves, vineyards, nurseries and ornamental horticultural areas 23 Confined feeding operations 24 Other agricultural land
3. Rangeland	31 Herbaceous rangeland 32 Shrub and brush rangeland 33 Mixed rangeland
4. Forest land	41 Deciduous forest land 42 Evergreen forest land 43 Mixed forest land
5. Water	51 Streams and canals 52 Lakes 53 Reservoirs 54 Bays and estuaries
6. Wetland	61 Forest wetland 62 No forested wetland
7. Barren land	71 Dry salt flats 72 Beaches 73 Sandy areas other than beaches 74 Bare exposed rock 75 Strip mines, quarries and gravel pits 76 Transitional areas 77 Mixed barren land
8. Tundra	81 Shrub and brush tundra 82 Herbaceous tundra 83 Bare ground tundra 84 Wet tundra 85 Mixed tundra
9. Perennial snow and ice	91 Perennial snowfields 92 Glaciers

The supervised classification, on the other hand, contains a learning process through training data. The training data should be collected from the image. The training data set should be consisting of all spectral bands to be used in classification, be representative of all the available spectral variability for a given class, be sufficient enough for effective learning and be distributed spatially in a balanced manner. The learning algorithms used in supervised classification can be grouped into five categories:

1. Probabilistic classification algorithms,
2. Machine-learning-based classification algorithms,
3. Artificial intelligence-based classification algorithms,
4. Decision three classification algorithms,
5. Fuzzy set-based classification algorithms.

The probabilistic classification algorithms mainly rely on extracting statistical information from the training data and finding a statistical measure as the indication of each pixel's/segment's similarity to every class. Then the class label having the similarity value is assigned to the pixel/region. Maximum likelihood classification is a typical and most frequently used one. Support Vector Machine (SVM) is among the most widely used **machine learning-based classification algorithms**. In this method, an optimum hyperplane that separate the two different classes from each other is obtained. A subset of training data, which is called support vectors, defines the hyperplane with maximum margin. It has been showed by Huang *et al*. (2002) and Pal and Mather (2005) that SVM performs better in RS applications than maximum likelihood classification. **Artificial Neural Networks (ANN)** forms the backbone of the artificial intelligence-based classification. The ANN determines the hidden relations and rules from the training data, which is also called learning **Fuzzy set-based classification algorithms** provide better treatment of uncertainties in the classification, which results in mixed classes or hardly separable classes. **Decision tree classification algorithms** are based on hierarchical division of image data for defined class hierarchies, which can manually be constructed by the user or automatically using statistical properties of the spectral bands (Düzgün and Demirel, 2011).

For the reliable classification output, the accuracy assessment should be considered carefully and the accuracy assessment is performed a set of data (**ground truth**). The ground truth data can be obtained from field studies, existing maps or higher resolution images. In accuracy assessment, the output classes and ground truth are compared. This comparison is systematically done with the help of so called **error matrix** (confusion matrix/contingency table). Error matrix also used for obtaining statistical measures of accuracy. The most widely used statistic is **Kappa statistic** which is obtained by using error matrix.

Change analysis involves comparing multi temporal images of the same site. The simplest method of change analysis is subtracting of rationing multi temporal images. The values close to one and zero in the resulting change image indicate unchanged pixels, for subtraction and rationing, respectively. For more sophisticated analysis change detection algorithms that compare processed multi temporal images like comparing vegetation indices, classification results and principle component analysis are used. Prior to any change analysis application, the following pre-image processing analyses should be performed in order to have a better change analysis accuracy (Düzgün and Demirel 2011.

1. Precise geometric rectification analysis is required for accurate spatial pixel matching between the images. Inadequate geometric rectification yields unchanged areas as if they are changed since the spectral values corresponding the same area will not be the same for the same pixel.

2. Atmospheric correction for all the images is necessary in order to eliminate atmospheric effects in the spectral values.

3. If the images for the two or more different dates do not have the same spatial resolution and/or spectral band combinations, they their spatial and spectral resolution should be matched by image enhancement and resampling methods.

The result of change analysis is usually given in the form of a change map and a change matrix. An overview of change analysis methods can be found from Singh (1989), Mas (1999) and Lu et al. (2004).

The digital surface and terrain model (DSM/DTM) of an area can be either obtained from stereo pairs of the same area with at least 60 % overlapping areas or from aerial or LIDAR data or from radar interferometry. DSM generation is mainly obtaining the terrain height for certain points on the image and interpolating the height values to create a continuous height surface.

Feature extraction is mainly extracting boundaries of specific features like built up, road, railroad, airport, etc. from the images. These algorithms are specifically developed for extracting each feature such as built up extraction algorithms, road extraction algorithms etc. and features are mainly the man-made objects (e.g. Wurm et al, 2011).

3.4. Software For VHR Data Analysis

The most commonly used software products are:

- ERDAS-LPS
- PCI-Geomatica
- ENVI-IDL
- Z/I
- GAMMA
- SARscape
- OSSIM (http://www.ossim.org/ OSSIM/OSSIMHome.html),
- ORFEO (http://www.orfeo-toolbox.org/otblive/),
- Multi- Spec (http://cobweb.ecn.purdue.edu/~biehl/MultiSpec/)
- IDIOT (http://srv-43-200.bv. tu-berlin.de/idiot)
- DORIS (http://doris.tudelft.nl/).
- Matlab
- Definiens eCognition
- BEAM (http://envisat/esa/int/beam)

ERDAS-LPS, PCI-Geomatica and ENVI-IDL, Z/I, Matlab, Definiens eCognition provide capabilities for processing optical, radar and lidar data with associated modules. GAMMA and SARscape are specifically designed for processing radar (microwave) images. OSSIM, ORFEO and BEAM are mainly for optical RS open source products, while DORIS and IDIOT are open-source software for processing of radar image. Recently, various GIS software also provides limited image analysis capabilities.

4. Relation Between Indicators and VHR Data Analysis

The relation between routine planning activity indicators defined in WP3 and VHR data requirements as well as data analysis types are summarized in Table 5. As Table 5 indicates, majority of the indicators can be extracted from classification of VHR data. There are various indicators related to stereo analysis of the VHR data. However, obtaining VHR data in stereo pairs may not be either available by the satellite sensors or may require very sophisticated image analysis tools and relatively expensive as compared to conventional VHR data. These problems limit the widespread use of such data in routine urban planning practice. Extraction of built ups and road networks are required for a few number of indicators which mainly requires feature extraction.

Table 5. Summary of routine planning activity indicators and their relation to VHR Data.

Sector	GEOURBAN indicators/parameters with relevance to EO	VHR Data Requirement	VHR Data Analysis
Air pollution and public health	AOT, Surface topography (DTM), built up structure (DSM), built-up density, population distribution as input for dispersion models and emission scenarios	Stereo Images for DTM and DSM generation Multispectral images with at least four image bands of R,G,B,NIR	Stereo image analysis for DSM and DTM Image classification for built-up density
Energy efficiency	Built up structure DSM , solar input	Stereo Images for DTM and DSM generation	Stereo image analysis for DSM and DTM

Water	sea/water surface temperatures, and temperature change, land cover , land cover change	Multispectral images with at least four image bands of R,G,B,NIR Multi temporal images for change detection	Image transformation for water and vegetation masks Classification for land cover Chance detection for land cover change
Transportation and mobility, accessibility	Traffic (street and railway) network, lines of communication	Multispectral images with at least four image bands of R,G,B,NIR	Feature extraction for road detection
Thermal comfort	surface temperatures, urban surface materials, surface albedo, surface emissivity, built up density, fractional land cover, imperviousness/surface sealing	Multispectral images with at least four image bands of R,G,B,NIR	Classification for land use and land cover, built-up density
Urban green	Land cover, urban surface materials, vegetation indices, fractional land cover	Multispectral images with at least four image bands of R,G,B,NIR	Image transformation for vegetation masks Classification for land use and land cover, built-up density
Territorial development	built up density, land cover, land cover change	Multispectral images with at least four image bands of R,G,B,NIR Multi temporal images for change detection	Classification for land cover Chance detection for land cover change
Vulnerability to environmental hazards	Surface topography(DTM), built-up density (DSM), population distribution, input for dispersion models, critical infrastructure	Stereo Images for DTM and DSM generation Multispectral images with at least four image bands of R,G,B,NIR	Surface Stereo image analysis for DSM and DTM Image classification for built-up density

5. VHR Data Analysis for Obtaining Indicators

In the light of Table 5, in the following subsections algorithms used for land use land cover (LULC) detection for urban areas and building and road detection are overviewed as they require single VHR data.

5.1. Land Use Land Cover (LULC) Classification

Among the various classification algorithms, Maximum likelihood classifier (MLC), neural network (NN) classifiers and decision tree classifiers are well-known and most widely used classifiers. The MLC is used with respect to statistical theory; however, neural networks are used with respect to non-parametric approach. As a result, many types of neural networks have been developed (Lippman 1987); the most widely used in the classification of remotely sensed images is a group of networks called a multi-layer perception (MLP) (e.g. Paola and Schowengerdt 1995, Atkinson and Tatnall 1997). A decision tree classifier divides the classification problem into smaller branches. Depending on the number of variables used at each branch of the tree, there are univariate and multivariate decision trees (Friedl and Brodley 1997). Univariate decision trees have been used to develop land cover classifications at a global scale (DeFries et al. 1998, Hansen et al. 2000). Though multivariate decision trees are often more compact and can be more accurate than univariate decision trees (Brodley and UtgoV 1995), they involve more complex algorithms and, as a result, are affected by the set of algorithm-related factors (Friedl and Brodley 1997).

The support vector machine (SVM) is another widely used LULC classification algorithm which represents a group of theoretically superior machine learning algorithms. SVM is found to be competitive with the best available classification methods, including neural networks and decision tree classifiers (Huang, et al, 2010). In Seetha and Muralikrishna (2008) summarizes the pros and cons of various machine learning classification algorithms used in LULC classification (Table 6 and Table 7).

Table 6. Pros and cons of machine learning classifiers in LULC classification (Seetha and Muralikrishna, 2008).

Machine Learning Algorithm	Benefits	Assumptions and / or Limitations
Neural Network	• can be used for classification or regression • able to represent Boolean functions (AND, OR, NOT) • tolerant of noisy inputs • instances can be classified by more than one output	• difficult to understand structure of algorithm • too many attributes can result in over fitting • optimal network structure can only be determined • by experimentation
Support Vector Machine	• models nonlinear class boundaries • over fitting is unlikely to occur • computational complexity reduced to quadratic optimization • problem • easy to control complexity of decision rule and frequency of • error	• training is slow compared to Bayes and Decision • trees • difficult to determine optimal parameters when • training data is not linearly separable • difficult to understand structure of algorithm
Fuzzy logic	• different stochastic relationships can be identified to • describe properties	• Priori knowledge is very important to get good • results. • precise solutions are not obtained if the direction of • decision is not clear
Genetic Algorithm	• can be used in feature classification and feature selection • primarily used in optimization always finds a “good” • solution (not always the best solution) • can handle large, complex, non differentiable and • multimodal spaces. • Efficient search method for a complex problem space. • good at refining irrelevant and noisy features selected for • classification.	• computation or development of scoring function is • nontrivial • not the most efficient method to find some optima, • rather than global • complications involved in the representation of • training/output data

Table 7. Comparison of machine learning algorithms used in LULC classification (Seetha and Muralikrishna, n.d.).

Parameter	Artificial Neural Networks	Support Vector Machines	Fuzzy logic	Genetic Algorithms
Type of approach	Non-parametric	Non-parametric with binary classifier	Stochastic	Large time series data
Non-linear decision boundaries	Efficient when the data have only few input variables.	Efficient when the data have more input variables.	Depends on Priori knowledge for decision boundaries	Depends on the direction of decision
Training speed	Network structure, momentum rate, learning rate, converging criteria.	Training data size, kernel parameter, class separability	Iterative application of the fuzzy integral	Refining irrelevant and noise genes
Accuracy	Depends on number of input classes.	Depends on selection of optimal hyper plane	Selection of cutting threshold	Selection of genes
General performance	Network structure.	Kernel parameter	Fused fuzzy integral	Feature selection

The total accuracy of the machine learning algorithms used in LULC classification for 24 training cases are illustrated in Figure 2.

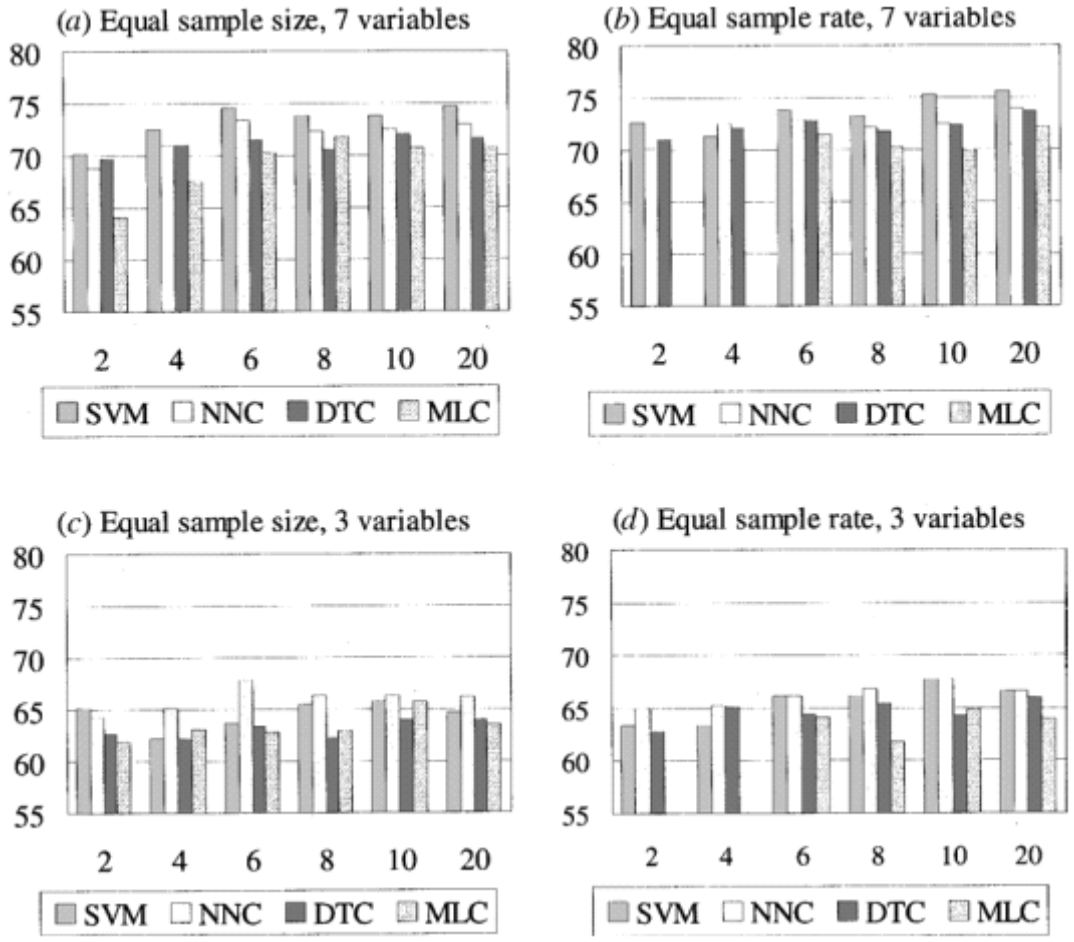

Figure 2. Overall accuracies of classifications developed using the four classifiers. Y-axis is overall accuracy (%). X-axis is training data size (% pixel of the image). (a) Equal sample size, 7 variables, (b) equal sample rate, 7 variables, (c) equal sample size, 3 variables, (d) equal rate, 3 variables. Huang et al. (2002).

The stabilities of the algorithms differed greatly and were affected by training data size and number of input variables. In general, the overall accuracies of the algorithms were more stable when trained using 20% pixels than using 6% pixels, especially when seven variables were used. The SVM gave far more stable overall accuracies than the other three algorithms when trained using 20% pixels with seven variables. It also gave more stable overall accuracies than the other three algorithms when trained using 6% pixels with seven variables (Figure 3(b)) and using 20% pixels with three variables (Figure 3(c)). (Huang et al., 2002)

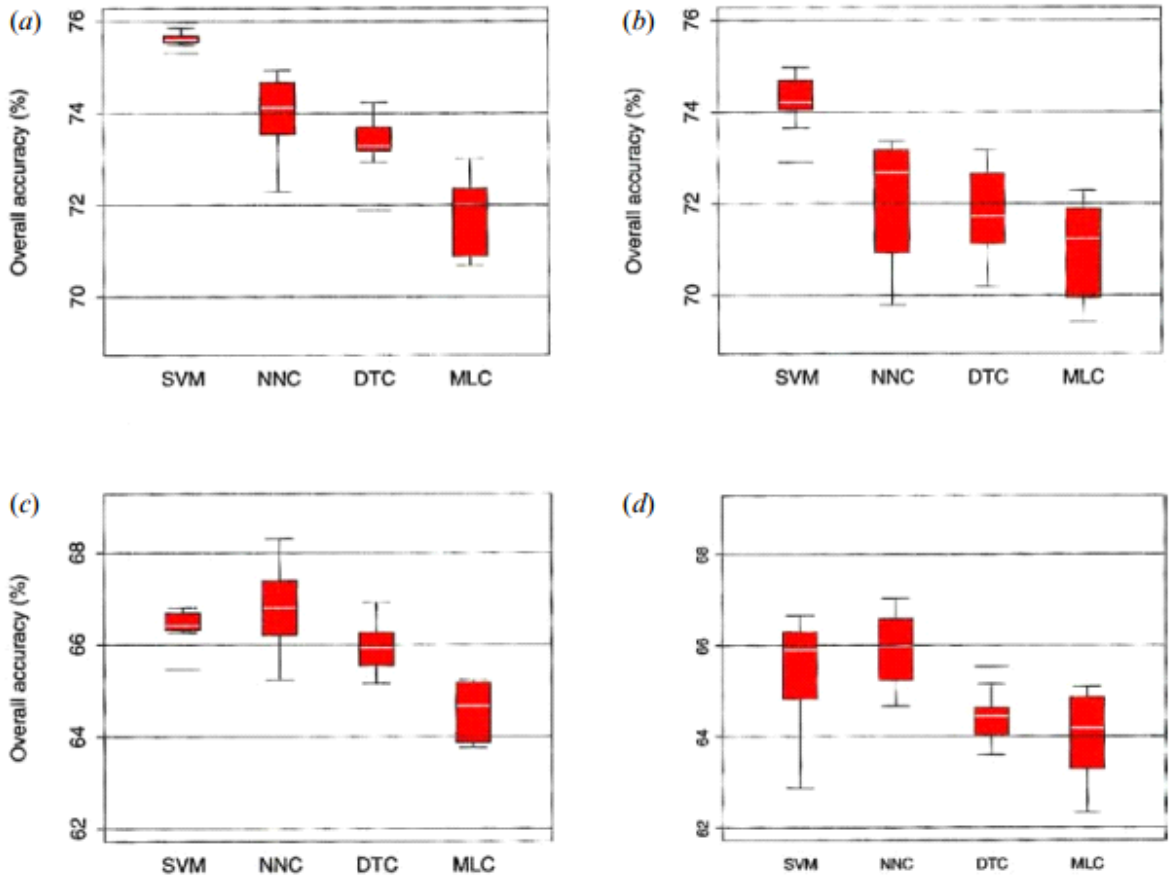

Figure 3. Boxplots of the overall accuracies of classifications developed using ten sets of training **samples randomly selected from the Maryland data set. (a). Training size= 20% pixels of the image, number of input variables=7. (b) Training size=6% pixels of the image, number of input variables=7. (c) Training size=20% pixels of the image, number of input variables=3. (d) Training size=6% pixels of the image, number of input variables=3.**

For VHR data, there are several approaches adopted in the literature to overcome insufficiency of spectral information, such as making use of textural features, shape information of target classes or embedding spatial information to get context involved. Recently, impressive performance results are obtained by combining pixel-based and object-based methods, which is called "hybrid" (Shackelford and Davis 2003, Aksoy et al. 2009, Wang et al. 2008, Tarabalka et al. 2010, Wang et al. 2005). In most of these studies, selection of a hierarchical or decision-tree-based approaches stands out (Aksoy et al., 2009, Shackelford and Davis, 2003, Wang et al., 2008). In (Aksoy and Akcay, 2005), a

multi-resolution approach is used and a decision tree classification which uses Gini index is reported to be more successful than a multivariate Gaussian classifier for 7 classes, namely, roof, street, path, grass, trees, water, and shadow. For LULC problem, decision trees are used even in the existence of partly missing data and shown to be able to fuse data from multiple sources successfully (Aksoy et al., 2009). It is also noted that decision trees are as good as other popular classifiers such as MLC, SVM, NN, etc. (Aksoy et al., 2009).

5.2. Building and Road Extraction

As the manual extraction of urban objects from VHR data requires qualified domain experts and a large amount of effort in terms of time and cost, resent building extraction algorithms focus on semi/automatic methods to increase the speed of this process However, due to the required accuracy and the involved complexity in the VHR data, semi- or fully automated building extraction methods are still in the process of improvement (Wilkinson 2005).

Extraction of urban objects like buildings and roads from high-resolution satellite data has mainly two different aspects. The first aspect is related to the object properties. Inherently, man-made structures are composed of different sizes and different surface materials such as concrete, brick, asphalt, metal, plastic, glass, shingles, soil etc. (Aytekin et al. 2012). Hence, there is a high spatial and spectral diversity. Usually urban environment involves complex features like various shapes and surface materials and buildings may appear indistinguishable from roads and pavements or vice versa. Also rooftops may reflect fragmented characteristics due to shading or they may be occluded by other buildings or vegetation. The second aspect is related to the image properties. Images differ in resolution, sensor type, orientation, quality, dynamic range, illumination conditions, weather conditions, seasons etc. (Aytekin et al.,2012). Thus, it is hardly possible to use a certain algorithm for all kinds of images and all types of urban objects lie buildings and roads. As a result, due to the complexity of the problem, there are various approaches for extraction of buildings and roads, which are still in the stage of improvement.

The early works in building detection were based on line extraction, edge detection and building polygon generation. These methods mostly use a large set of heuristic rules and are computationally expensive. Typical examples of these methods are Herman and Kanade (1986), Huertas and Nevatia (1988), Irving and McKeown (1989),Matsuyama and Hwang (1990), Venkateswar and Chellappa (1991), Krishnamachari and Chellappa (1996), Lin and Nevatia (1998), Kim and Nevatia (1999),Mayer (1999), Gereke et al. (2001), Persson et al. (2005) and Peng and Jin (2007). The studies of Muller et al. (1997), Baltsavias et al. (2001) and Sohn and Dowman (2001) extensively discuss the effect of resolution on the building extraction.

The existing approaches related to automatic/semi-automatic extraction of buildings from VHR data can be divided into two main categories. The first category relies on the classification of the objects using multispectral reflectance values (e.g. Segl and Kaufmann 2001, Shan and Lee 2002, Benediktsson et al. 2003, Lee et al. 2003, Ünsalan and Boyer 2005, Sohn et al. 2005, Katartzis and Sahli 2008; Taubenböck et al., 2010). The second category is mainly based on feature extraction techniques from panchromatic (PAN) images (e.g. Lin and Nevatia 1998, Wei et al. 2004, Wei and Prinet 2005).

In general, building extraction from VHR data involves two phases. In the first phase the region of interest (RoI) i.e. urban built-up areas which contain building foot print is obtained. Then in the second phase, buildings based on feature extraction and classification algorithms are obtained. In the literature, different kinds of features were defined and feature spaces were created (Pesaresi 2000, Benediktsson et al. 2001, Tatem et al. 2001, Haverkamp 2004, Zhen et al. 2004). These features were either classified if supervision is available or clustered if supervision is not possible.

The features of building extraction which are widely used in the literature can be grouped as geometric, specktral and structural. Geometric features define basic geometrical properties such as area, circumference, roundness, right angles, corners, straight lines etc. Spectral features are related to color or band information. Structural features refer to connectedness of neighbors according to some similarity measures.

Classification of the content was generally performed by the rule-based and the context-driven approaches and the content was classified into several types such as buildings, vegetation, roads and water areas. In doing this, density (rural, suburban, urban), object complexity (residential, industrial, military), architecture (elaborate, plain,

none), terrain defined by digital elevation model (DEM) (flat, hilly, mountainous) or vegetation defined by Normalized Difference Vegetation Index (NDVI) (none, moderate, heavy) were taken into account.

Some studies are concentrated on extracting low-level features from model-based context-driven hypothesis and subsequently set relations among them in favor of supporting the building hypothesis (Haverkamp 2004, Zhen et al. 2004, Peng and Liu 2005, Katartzis and Sahli 2008, Lizarazo and Elsner 2009).

Multi-scale analyses are also studied in the literature (Huang et al. 2007, Chen et al. 2009). Most of the works in the literature concentrates only on the extraction of a single object such as only buildings or only roads. They do not consider road extraction and building extraction together. Aytekin et al. (2012) proposed a generic algorithm for automatic extraction of buildings by considering the roads as well.

Besides buildings, road extraction is also considered in semi- or fully automated object detection from VHR data. Mostly snakes, higher order active contours, dynamic programming or probabilistic approaches have been proposed for road detection. For example, Klang (1998), Laptev et al. (2000) and Peteri and Ranchin (2003) used the most common snake's algorithm for the detection of road. Mena and Malpica (2003) and Guo et al. (2004) focused on segmenting road areas. Guo et al. (2004) dealt with investigating on how to build geo-specific road databases from aerial images for driving simulation. Mena and Malpica (2003) used the Dempster-Shafer theory of evidence for the fusion of texture to extract linear features. Amini et al. (2002) proposed a fuzzy logic algorithm for road extraction from multispectral imagery. Barzohar and Cooper (1996) used dynamic programming and Bicego et al. (2003) proposed probabilistic approaches for road detection. Bacher and Mayer (2005) introduced an approach for automatic road extraction from high-resolution multispectral imagery; Christophe and Inglada (2007) proposed a robust geometric method to provide a first step extraction level of road; and Yang and Wang (2007) proposed an improved model for road detection based on the principles of perceptual organization and classification fusion in human vision system (HVS).

Topology, parametric models, snakes, and semantic networks are the most popular road representation methods. Table 8 summarizes methodologies and image resolution used for road extraction. As it can be seen from Table 8, as well as various images

obtained from different RS platforms, the spatial resolution of the images used for road extraction ranges from 0.5 meters to 75 meters.

Table 8. Road detection methods and used spatial resolution

Previous Research	Resolution (m)	Methodology
Bajcsy and Tavakoli (1976)	79	topology
Wang and Newkirk (1988)	10	semantic network
Fiset and Cavayas (1997)	30	topology, tracking
Netanyahu et al. (1997)	1-3	parametric
Tupin et al. (1998)		semantic network
Karathanassi et al. (1999)	6.25, 10	topology, parametric
Laptev et al. (2000)	0.5	snakes
Jeon and Hong (2002)		grouping, snakes
Shi and Zhu (2002)	1	topology
Stoica et al. (2004)	5	point processes
Mena and Malpica (2005)	0.5	texture
Zhang and Couloigner (2006)	1	texture
Hu et al. (2007)	1	tracking
Yang and Wang(2007)	1	perceptual organization
Peng et al. (2008)	0.6	variational model
Movaghati et al. (2010)	1	particle, Kalman filtering

5.3. Change Analysis

As most of the indicators involve analysis of changes in urban areas, detecting changes from multi-temporal VHR data is a valuable tool. Obtaining appropriate change analysis relies on spatial, temporal, spectral and radiometric properties of VHT data. The following conditions should be satisfied for an effective change analysis (Jensen *et al.,* 1997, Lunetta and Elvidge, 1998, Coppin *et al.,* 2004, Millward *et al.,* 2005):

- ✓ VHR data from the same satellite sensor should be obtained if the image differencing or rationing approaches will be used so that the change analysis does not affected by the radiometric differences. Considering the issues related to spatial resolution, VHR data from the same satellite sensor is also useful for less effort of geometric correction.
- ✓ The images obtained from different years should be from the similar time of year or similar season or month to be least affected by the solar illumination angle effects and to minimize differences in seasonal land cover like vegetation, water.
- ✓ VHR data of different dates should be registered to each other or orthorectified with an accuracy of 0.5 pixel of 0.5 RMSE (Root Mean Square Error) so that change analysis does not affected by spatial distortions.
- ✓ Each VHR data should be normalized radiometrically in order to minimize atmospheric effects.

As change analysis has one of the widest application areas of RS, literature is abundont. Pape (2006) summarized existing change detection methods (Table 9) by refering to Singh (1989), Coppin and Bauer (1996), Lunetta and Elvidge, (1998), Yuan *et al.,* (1998), and Coppin *et al.,* (2004)

Table 9. Summary of change detection approaches (After Pape, 2006)

Change Analysis Method	Description of the Method	Pros	Cons
Post-classification Comparison	Independently produce spectral classification and then compare multi temporal classifications pixel-by-pixel	-No radiometric processing required - No post change classification required	-Results dependent on accuracy of original classification
Composite Analysis	Statistical difference determined using multistage decision logic	- Necessitates only a single classification	-Very complex especially for multiple dates - Demands prior knowledge of logical interrelationships of the classes - Difficulty in class labelling
Univariate Image Differencing	Subtraction of multi temporal imagery, original or transformed data	- Widely adopted - Simple	-Requires precise registration - Highly dependent on change/no change thresholding technique
Image Ratioing	Pixels are ratioed, no change ratio = 1	-Simple	Criticized as being statistically invalid (Riordan, 1981)
Bi-Temporal Linear Data Transformation	Applied to two-date imagery to produce uncorrelated data. Most widely used ones are PCA and Tasselled Cap	- Simple - Very effective	- PCA requires comprehensive knowledge of study area
Change Vector Analysis	Multivariate change detection that processes the full dimensionality of the image data and produces two outputs: change magnitude and change direction	- Analyzed change concurrently in all data layers - Highly effective	- Requires perfect registration - Intensive user interaction
Image Regression	Mathematical model that describes the fit between through step-wise regression - Assumes a linear relationship between multitemporal no change data	- Regression techniques also account for atmospheric conditional and sun angle	-Threshold definition critical - Report accuracies similar to univariate image differencing but more complex
Multitemportal Spectral Mixture Analysis (MSMA)	Based on differences in high spectral resolution end member	- detect very fine detailed change (i.e. thinning of forests)	Requires high spectral resolution imagery - Provide physically-based, standardized measures of fractional abundance

6. VHR SAR Data Analysis for Obtaining Indicators

In contrast to passive optical sensors, radar systems are active imaging devices capable of acquiring data both during day and night independently from weather or environmental conditions.

SAR systems operate at a single wavelength or frequency, hence the appearance of different objects in SAR images is rather determined by geometrical and dielectric properties of the illuminated objects rather than by their biophysical or chemical characteristics as in case of optical data. In particular, most important factors influencing the radar backscatter are system-specific imaging parameters such as frequency-wavelength ratio, polarization and imaging geometry, object-specific imaging parameters (e.g., surface roughness) as well as terrain and object geometry (Esch et al., 2012).

SAR sensors used to have a reputation as being unsuitable for a precise thematic characterization of the urban environment (Dell' Acqua, 2010). Nevertheless, this has changed with the emergence of the latest-generation SAR sensors such as TerraSAR-X, Tan-DEM-X RADARSAT-2, CosmoSkyMed or ALOS-PALSAR and the resulting operational availability of VHR SAR data.

Different studies have shown that radar imagery is an excellent basis for classifying, monitoring and analyzing urban settlements and their development over time, especially in cases of large area mapping (e. g. Dell'Acqua & Gamba, 2003; Dell'Acqua, 2009). Object-oriented concepts for urban SAR data analyses have been recently presented in the literature (Matikainen et al. 2006; Esch et al. 2010) together with methods for deriving single built-up structures and areas experiencing built-up reconstruction from VHR radar data (Thiele et al., 2007). Grey and Luckman (2003) also introduced the use of interferometric coherence derived from ERS data for mapping urban extent. Furthermore, approaches for data fusion of SAR imagery and optical or LIDAR data have been also investigated (Gamba et al., 2006). A comprehensive overview on methods and applications of radar RS of urban areas is provided by Soergel (2010).

6.1. Monitoring Urban Land Surface Deformations

Monitoring urban settlements by means of SAR data represents one of the major topics in radar RS. In this context, spaceborne radar interferometry (InSAR) has already proven its great potential for detecting and quantifying ground deformations (e.g., due to mining or underground construction activities, earthquakes or volcanic processes) with a theoretical precision in describing the ground displacement up to a few millimeters (Colesanti et al, 2003). The most promising InSAR method in an urban context is the Permanent Scatterers Synthetic Aperture Radar Interferometry (PSInSAR) (Ferretti et al. 2000, 2001). In particular, instead of extracting information from the entire SAR image, PSInSAR exploits long temporal series of data to identify point-like stable reflectors, whose electromagnetic stability allows obtaining around 1-meter-accuracy DEM (Pesissin and Ferretti, 2007) and millimetric estimates of terrain motion (Ferretti et al. 2007). Usually PSs correspond to man-made targets, making the application of PSInSAR technology particularly suitale for urban areas (Pesissin and Ferretti, 2007).

6.2. Monitoring Urban Land Cover

Esch et al. (2010, 2011) demonstrated the suitability of VHR SAR data for detecting and delineating urban settlements by means of textural information and proposed a classification procedure including a texture estimation process in combination with the analysis of the backscattering characteristics of the SAR images. The classification process results in a binary mask discriminating between built-up areas and non-built-up areas, i.e. the so called Urban Footprint (UF), with overall accuracies ranging between 70% and 95%, depending on the geographical area. Into details, the texture analysis is carried out by comparing the local image heterogeneity to the fading texture (i.e., the scene-specific level of heterogeneity induced by speckle). This allows to derive a texture layer exhibiting very high values in correspondence of built-up areas (for which the difference between the two quantities is more pronounced), which is used together with the original backscatter intensity information to detect urban areas.

6.3. Digital Elevation Model Retrieval

Digital elevation models (DEMs) are the basis for several applications and represent a paramount source information in urban applications (provided that the spatial accuracy is sufficiently high, as in the case of the DEM retrieved by means of TerraSA-X and TanDEM-X data which is generated at 12m resolution, Wessel et al. 2008). The data sources used for the DEM processing can be manifold (Li et al., 2005). In this framework, multitemporal SAR images acquired from displaced vantage points provide the basis for calculating the DEM of a certain area. The generation of a DEM starts from the unwrapping of the interferometric phase and involves the conversion to terrain height and the transformation from slant-range coordinates to an Earth-related reference frame (Rufino et al., 1998). The basic idea is to find the intersection between two curves:

- The interferometric phase, which has a monotonous (decreasing or increasing) behavior as a function of range time;
- The geometric phase, linking the interferometric phase to the height of one object on the Earth. This phase can be related to range time, as a vertical straight line of increasing terrain height crosses the circles of constant range delays, and it is monotonous as well, (with a trend opposite to the interferometric phase), intersecting thus the first one.

7. Case Studies

7.1. LULC Classification for Basel

Since many of the identified indicators can be derived from land use land cover (LULC) maps, in this study LULC classification for a selected site of Basel is presented. To this aim one 4 band (R,G,B,NIR) Quickbird Multispectral image with a 2.51 m spatial resolution is considered (Figure 4). In particular, the study area covers a part of the central business district with dense built up and road features.

Figure 4. Quickbird image of the study area

A flow chart of the LULC algorithm implemented for this case study is given in Figure 5.

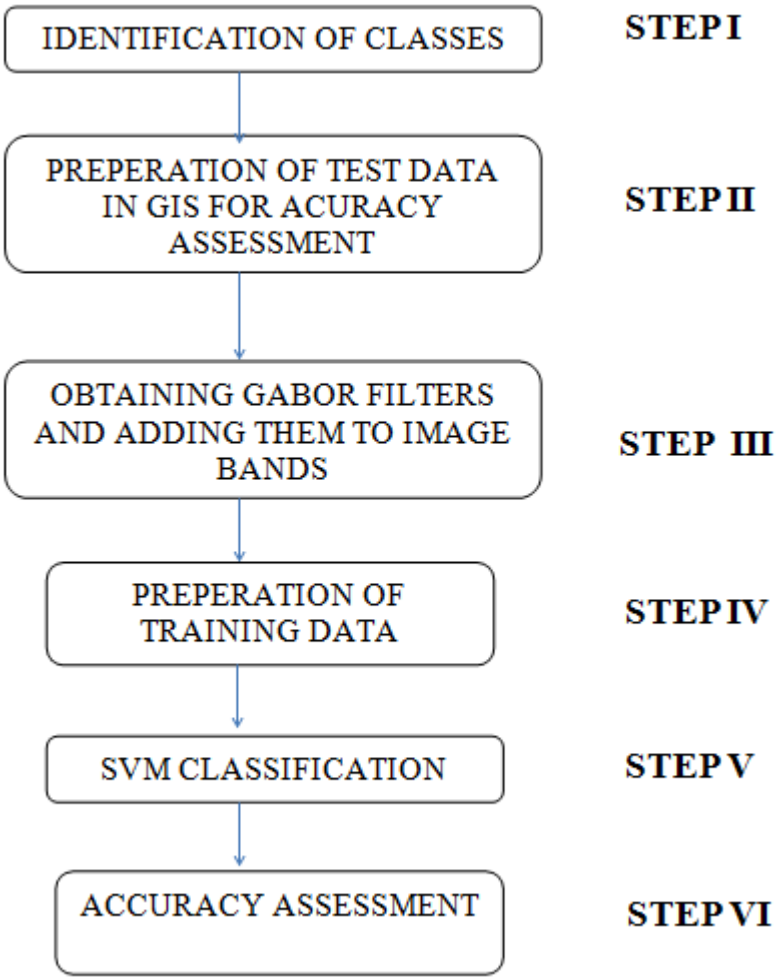

Figure 5. Flowchart of the applied classification methodology.

The first step consists in the visual investigation of the image since every LULC classification algorithm requires a reliable identification of the different information classes in the region of interest. Six major classes have then been identified, namely water, grass, trees, bare land, roads and built-up areas. In the second step is preparation of a point vector layer to test the classification accuracies by using GIS software. 330 points which are proportional to the each LULC class, is generated manually (Figure 6). Figure 6 represents the distribution of the test data on the study area.

Figure 6. Spatial distribution of the test data for accuracy assessment.

Due to dense build-up area concentration of the study area (Figure 4), Gabor filters, which provide good information about man-made linear objects (Bayram et al., 2011a and 2011b), are added as additional image bands to the multispectral data (Step III). Gabor filters in eight directions for each image band are obtained. Then each set of eight Gabor filters for four image bands (i.e.32 Gabor filters on total) are reduced to one maximum Gabor response image for four multispectral bands. Finally the Gabor maximum response images are added as additional four bands to the original image bands (Figure 7). Gabor filters are obtained by running Matlab codes. An example Gabor filter code in Matlab environment can be found from http://www.mathworks.com/matlabcentral/fileexchange/23253-gabor-filter/content/Gabor%20Filter/gabor_example.m and listed below:

```
function gabor_example()
% an example to demonstrate the use of gabor filter.
% requires lena.jpg in the same path.
% the results mimic:
% http://matlabserver.cs.rug.nl/edgedetectionweb/web/edgedetection_examples
% .html
% using default settings (except for in radians instead of degrees)
%
% note that gabor_fn only take scalar inputs, and multiple filters need to
% be generated using (nested) loops
%
% also, apparently the scaling of the numbers is different from the example
% software at
% http://matlabserver.cs.rug.nl
% but are consistent with the formulae shown there
lambda  = 8;
theta   = 0;
psi     = [0 pi/2];
gamma   = 0.5;
bw      = 1;
N       = 8;
img_in = im2double(imread('lena.jpg'));
img_in(:,:,2:3) = [];   % discard redundant channels, it's gray anyway
img_out = zeros(size(img_in,1), size(img_in,2), N);
for n=1:N
    gb = gabor_fn(bw,gamma,psi(1),lambda,theta)...
        + 1i * gabor_fn(bw,gamma,psi(2),lambda,theta);
    % gb is the n-th gabor filter
    img_out(:,:,n) = imfilter(img_in, gb, 'symmetric');
    % filter output to the n-th channel
    theta = theta + 2*pi/N;
    % next orientation
end
figure(1);
imshow(img_in);
title('input image');
figure(2);
img_out_disp = sum(abs(img_out).^2, 3).^0.5;
% default superposition method, L2-norm
img_out_disp = img_out_disp./max(img_out_disp(:));
% normalize
imshow(img_out_disp);
title('gabor output, L-2 super-imposed, normalized');
```

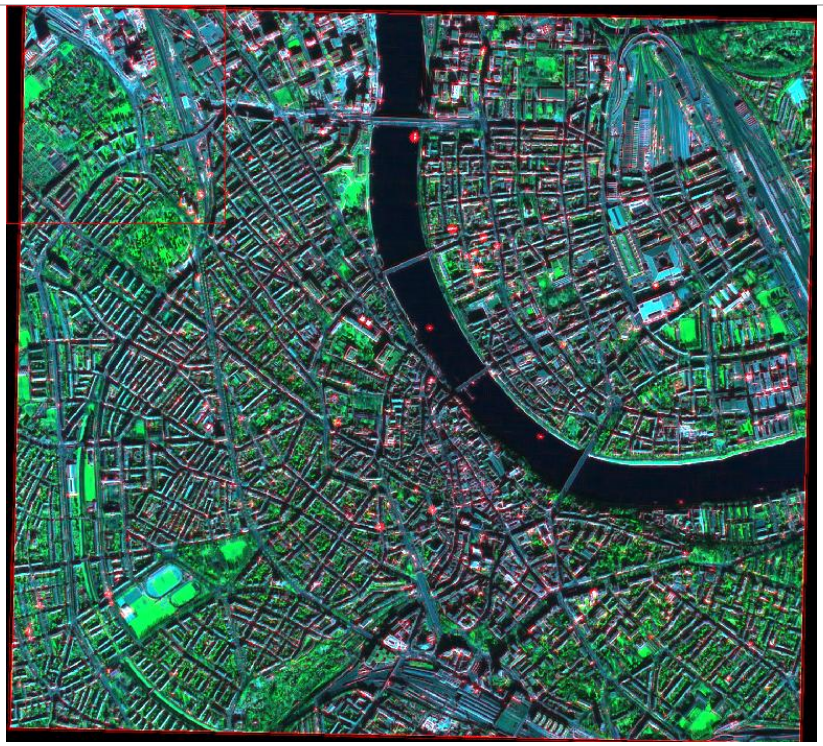

Figure 7. Input image of classification with eight bands (R,G,B, NIR and maximum Gabor responses of R,G,B, NIR).

In Step IV, training data for the LULC classes are obtained to be used in SVM. Visual investigation of the VHR data indicates that the study area contains building roofs with various roof material in grey, blue, white color as well as brick roofs. Hence training set is established for classes of road, water, grass, tree, bare land and four different roof types. The four different building roof material is later combined in a single building class during post processing of SVM output. The training set for SVM classification is illustrated in Figure 8.

Figure 8. Training data of the SVM classification.

Collection of the training data is carried out by using region of interest (RoI) tool of the ENVI. **Figure 9** and Figure 10 show the use of RoI tool in ENVI. The training data could be selected pixels or manually generated polygons. Once the training set for every class is obtained separability values should be calculated by using ROI tools of the ENVI software again. Separability values change in a range of 0 and 2. Larger values represent clear separation between related class combinations. **Figure 11** represents the use of the tool a and a separability output.

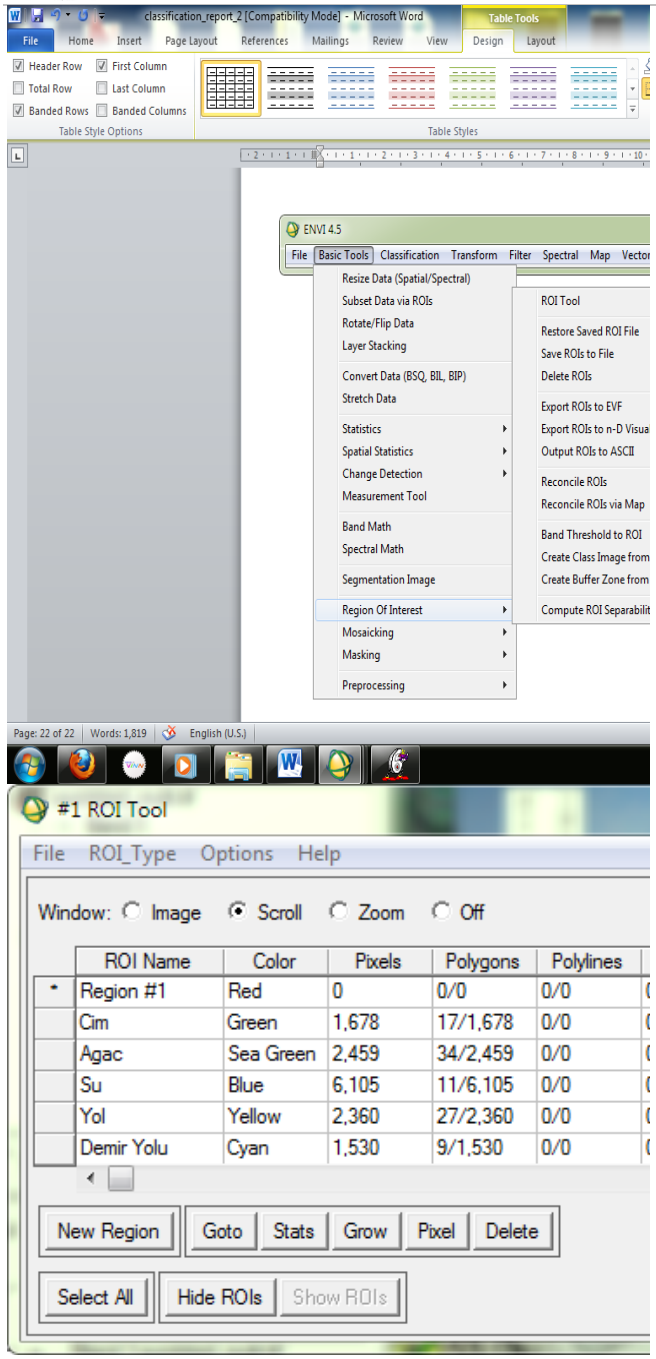

Figure 9. Use of RoI tool in ENVI

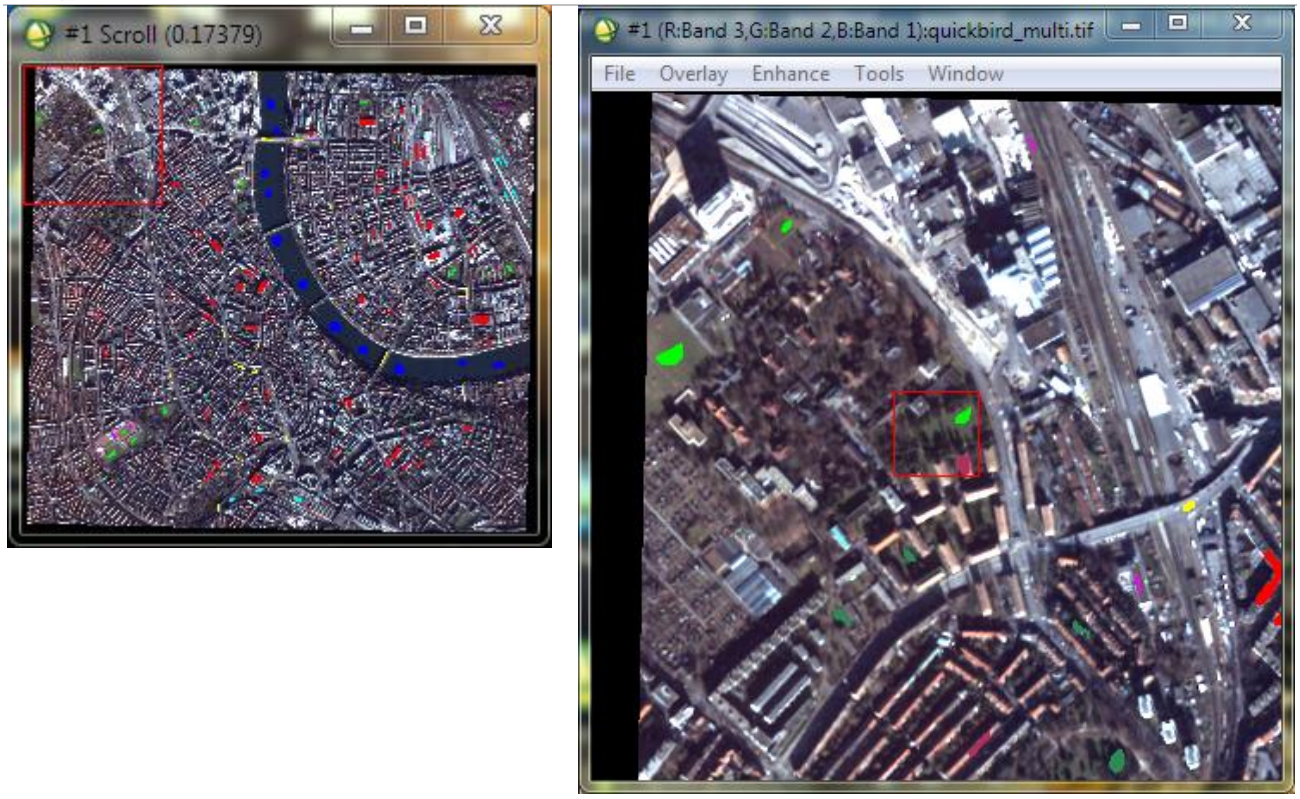

Figure 10. RoI tool interfaces of ENVI in the training data collection.

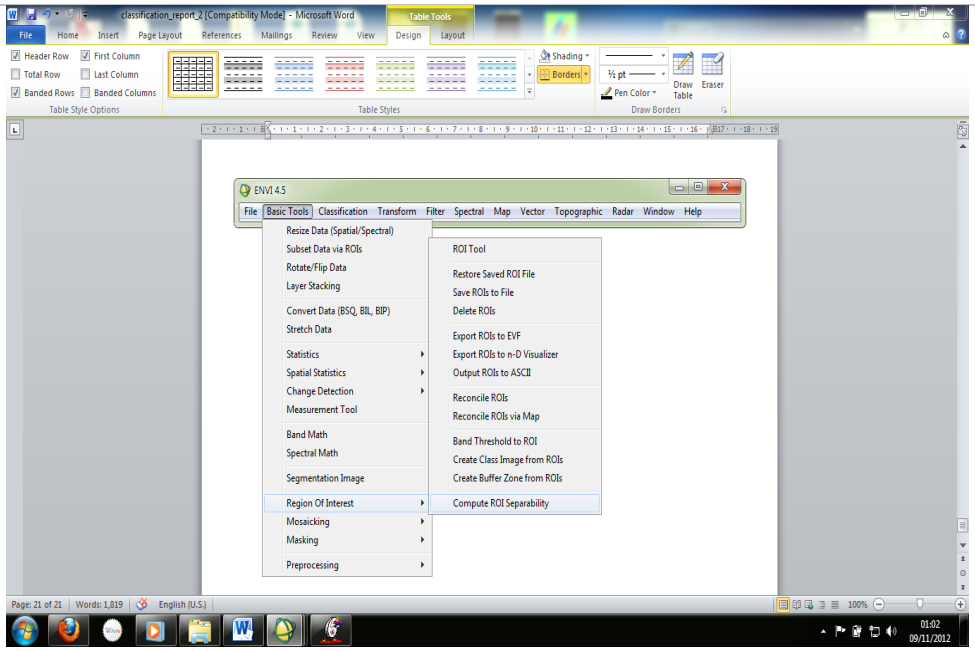

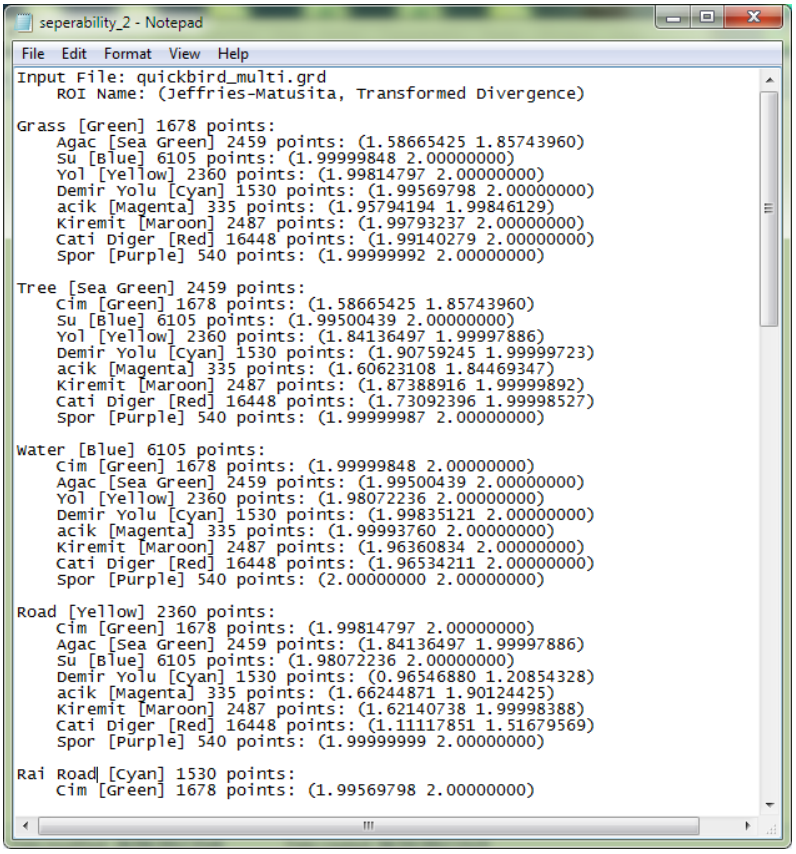

Figure 11. An example separability output of the ENVI

After collection of the training data and checking separability values of the classes, Step V, classification is performed by using Support Vector Machine (SVM) classification tool of the ENVI (Figure 12). Use of SVM tool of ENVI is illustrated in Figure 13.

Figure 12. LULC classification for the study area

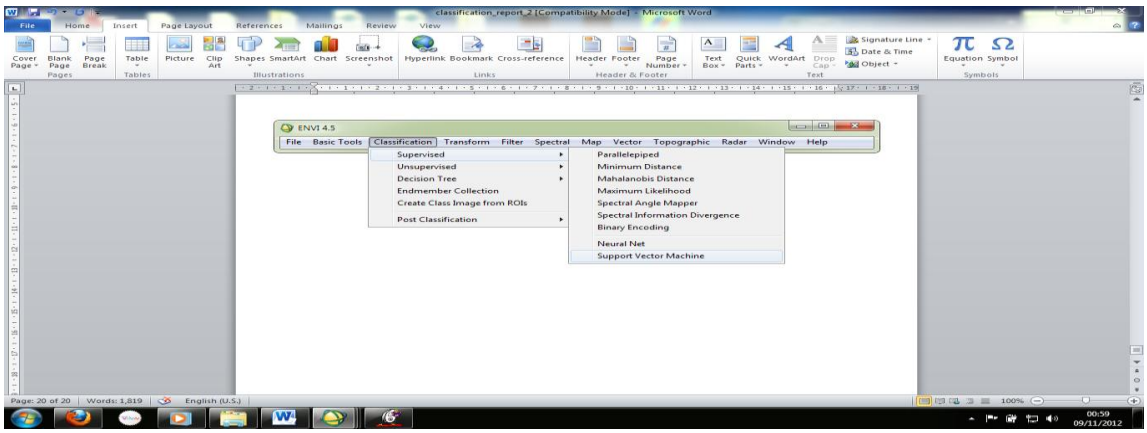

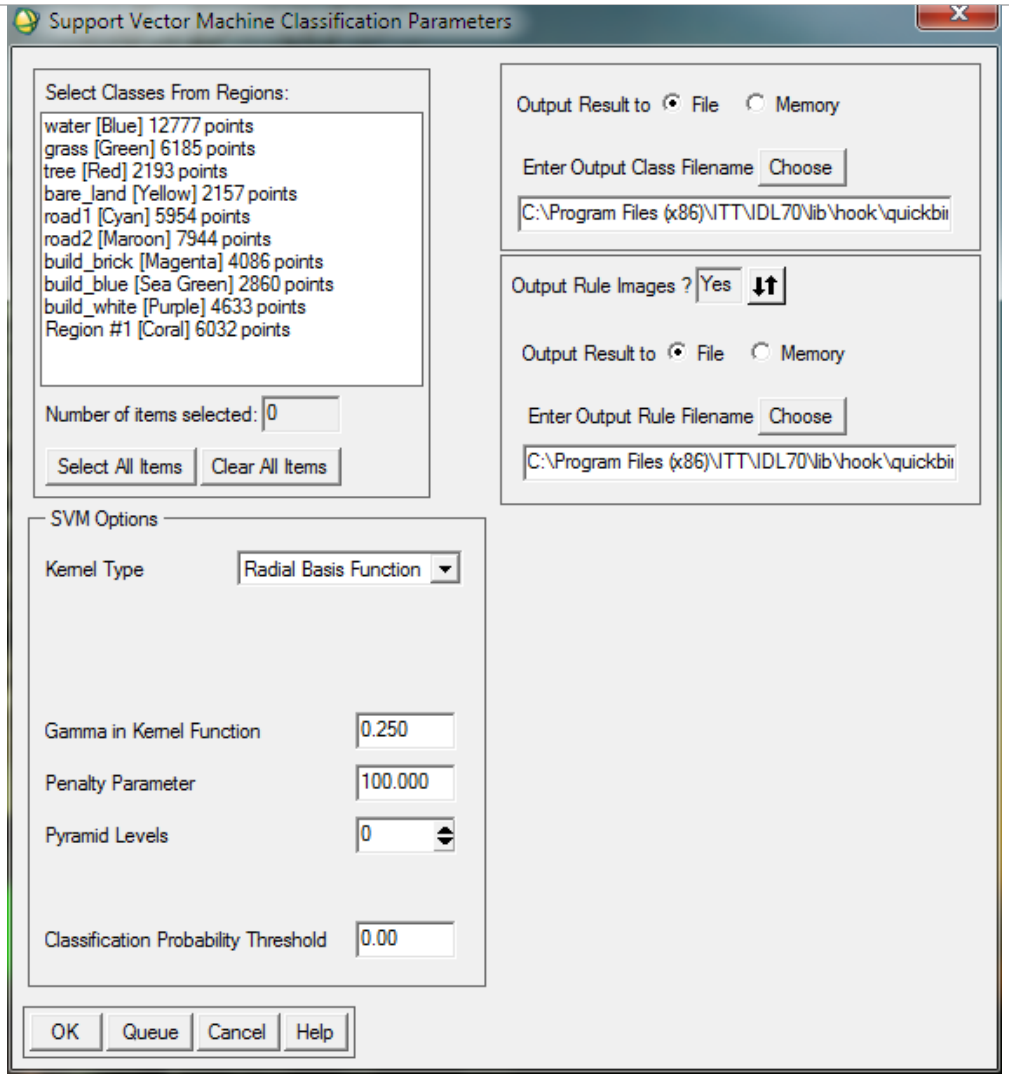

Figure 13. Use of SVM tool of ENVI .

The quality of the final LULC classification product in Figure 12 is evaluated by using accuracy measures of separation index, producer's accuracy, user's accuracy, overall accuracy and kappa coefficient. In Table 10 class separation index values are given for every class pairs. The lowest separation index is obtained for road and building as these urban features have similar radiometric properties in four of the multispectral bands as well as the Gabor responses. The separation index values are maximum for the pairs of natural and man-made classes.

Table 10. Pair separation index .

Class Pair	Separation Index	
Road	Building	0.73
Bare Land	Road	1.26
Tree	Bare Land	1.34
Tree	Road	1.39
Bare Land	Building	1.66
Road	Building	1.70
Bare Land	Road	1.80
Bare Land	Building	1.82
Tree	Building	1.83
Grass	Tree	1.89
Tree	Building	1.94
Tree	Road	1.95
Grass	Bare Land	1.96
Tree	Building	1.99
Water	Road	1.99
Water	Bare Land	1.99
Grass	Road	1.99
Grass	Building	1.99
Water	Tree	1.99
Water	Building	2.00
Grass	Building	2.00
Water	Road	2.00
Water	Grass	2.00

The accuracy measures for each class are given in Table 11. The overall accuracy and Kappa coefficient is found to be 0.75 and 0.62, respectively. Accuracy measures given in Table 11 indicates that even for a complex scene considered as the study area, water, grass and Building classes have high accuracy values. Although the other classes' accuracy values are less than water, grass and Building, they can be considered to be

satisfactory for deriving indicators from VHR satellite data. Building roof material with shadows in a dense built environment is the main problem in classification. Additional information (spatial, spectral etc.) could provide significant improvements in classification.

Table 11. Accuracy measures for each class .

Measure	Water	Grass	Tree	Road	Bare Land	Building
Producer's Accuracy	0.94	0.89	0.4	0.83	0.37	0.78
User's Accuracy	0.94	0.83	0.6	0.43	0.59	0.93

For the classification of TerraSAR-X data, a pixel-based classification algorithm has been employed (Esch et al., 2010). In particular, the proposed methodology includes a specific pre-processing of the original SAR backscattering amplitude for extracting suitable texture information followed by an automated threshold-based image analysis procedure which accounts for both the original backscatter amplitude image and the computed texture.

The pre-processing phase aims at extracting texture information capable of highlighting regions characterized by highly structured and heterogeneous built-up areas. This is carried out by taking advance of the specific characteristics of SAR data which exhibit strong scattering due to double bounce effects in urban areas. Accordingly, focus is given on the analysis of local speckle, whose development is estimated by means of the local image heterogeneity C_S defined as:

$$C_s \frac{\sigma_s}{\mu_s} \quad (1)$$

where, for each pixel, μ_S and σ_S represent the mean and the standard deviation of the backscatter amplitude, respectively, computed in a local neighborhood.

It is possible to prove that the following relationship exists between the image heterogeneity C_S, the true image texture C_T and the so-called fading texture C_F representing the heterogeneity caused by speckle:

$$C_s^2 = C_T^2 C_F^2 + C_T^2 + C_F^2 \quad (2)$$

Textured surfaces (e.g., urban environments, woodlands) are characterized by distinct structures, which lead to high C_T and C_F and hence to high values also for C_S. In turn, homogeneous surfaces without any true structuring (e.g., grasslands, non-cultivated bare soil) show almost no true texture C_T, meaning that C_S more or less equals the fading texture C_F which results in very low values being the backscatter almost randomly distributed.

In order to define a robust measure to describe the true image texture C_T we take into account this specific behavior. In particular, we consider the difference between measured local image heterogeneity C_S and scene-specific heterogeneity C_F and we assume that the true local texture C_T increases with a rising amount of real structures within the resolution cell. Accordingly, the local true image texture C_T is estimated as:

$$C_T = \frac{C_S - C_F}{1 + C_F} \quad (3)$$

Regions exhibiting highest values of (referred to as “speckle divergence texture”) correspond to urban areas, whereas open areas such as grasslands or water bodies are characterized by lower values.

The brightest regions in the image correspond with urban areas, while a low speckle divergence characterizes open areas such as grassland or water bodies (compare Figure 14 middle).

The speckle divergence feature serves then as input to the classification procedure together with the original backscatter amplitude image. The process starts with the identification of potential urban scatterers (the so-called “urban seeds”), which correspond to man-made structures with a vertical component (i.e., strong scattering due to double bounce) and are characterized by both high backscattering amplitude and high speckle divergence. This is carried out by comparing the locally (i.e., computed on a 15x15 pixel neighborhood) and regionally (computed on a 45x45 pixel neighborhood) averaged against two thresholds. In case one of the thresholds is exceeded, the region is classified

as a distinct backscattering cluster (DBC). It is worth noting that the thresholds are set in a way that only pixels with a very high local or regional deviation from C_F are assigned as DBC (Esch et al., 2012; Taubenböck et al., 2012).

In a second classification step all regions exhibiting both a certain amount of DBC in a neighborhood of 99x99 pixels and a regionally increased (i.e., on the basis of two additional thresholds) are categorized as built-up areas. The outcome represents the final urban footprint imagery, which is reported for the case studies Basel (**Figure 15Hata! Başvuru kaynağı bulunamadı.**), Tjumen (**Figure 15Hata! Başvuru kaynağı bulunamadı.**, left) and Tel Aviv (**Figure 15,Hata! Başvuru kaynağı bulunamadı.** right).

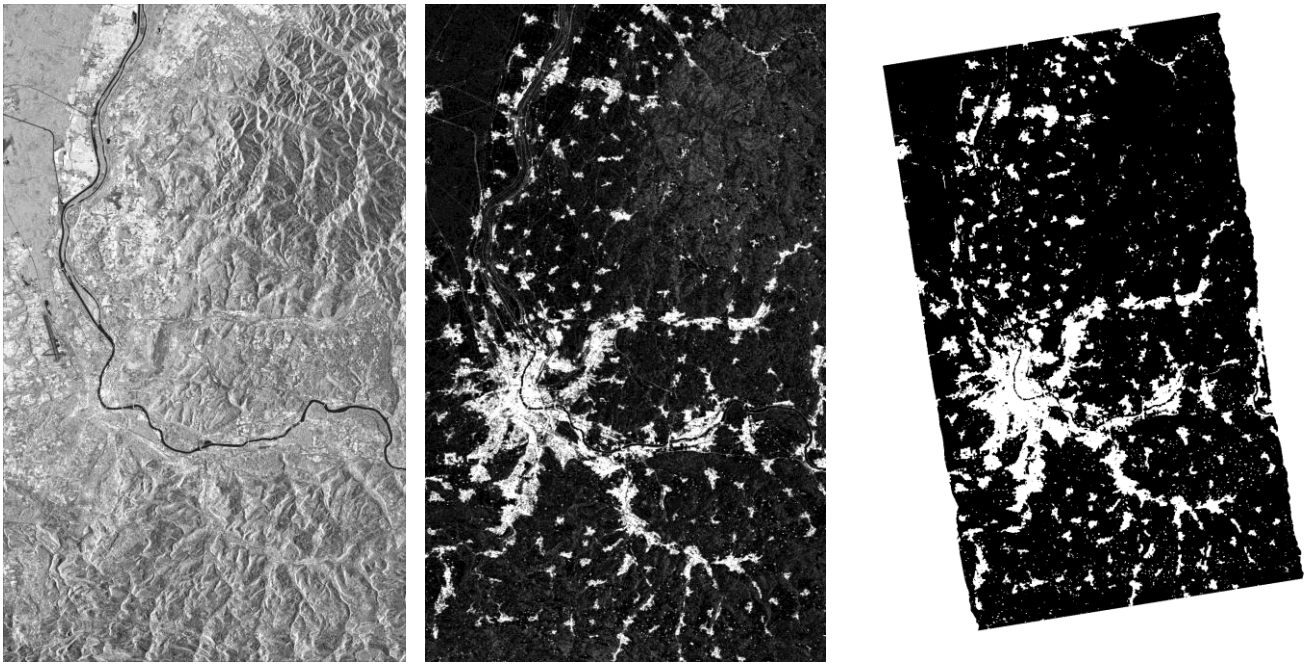

Figure 14. TSX backscattering amplitude image of Basel, Switzerland (left); speckle divergence feature derived from backscattering amplitude data (middle) and geocoded urban footprint classification (right).

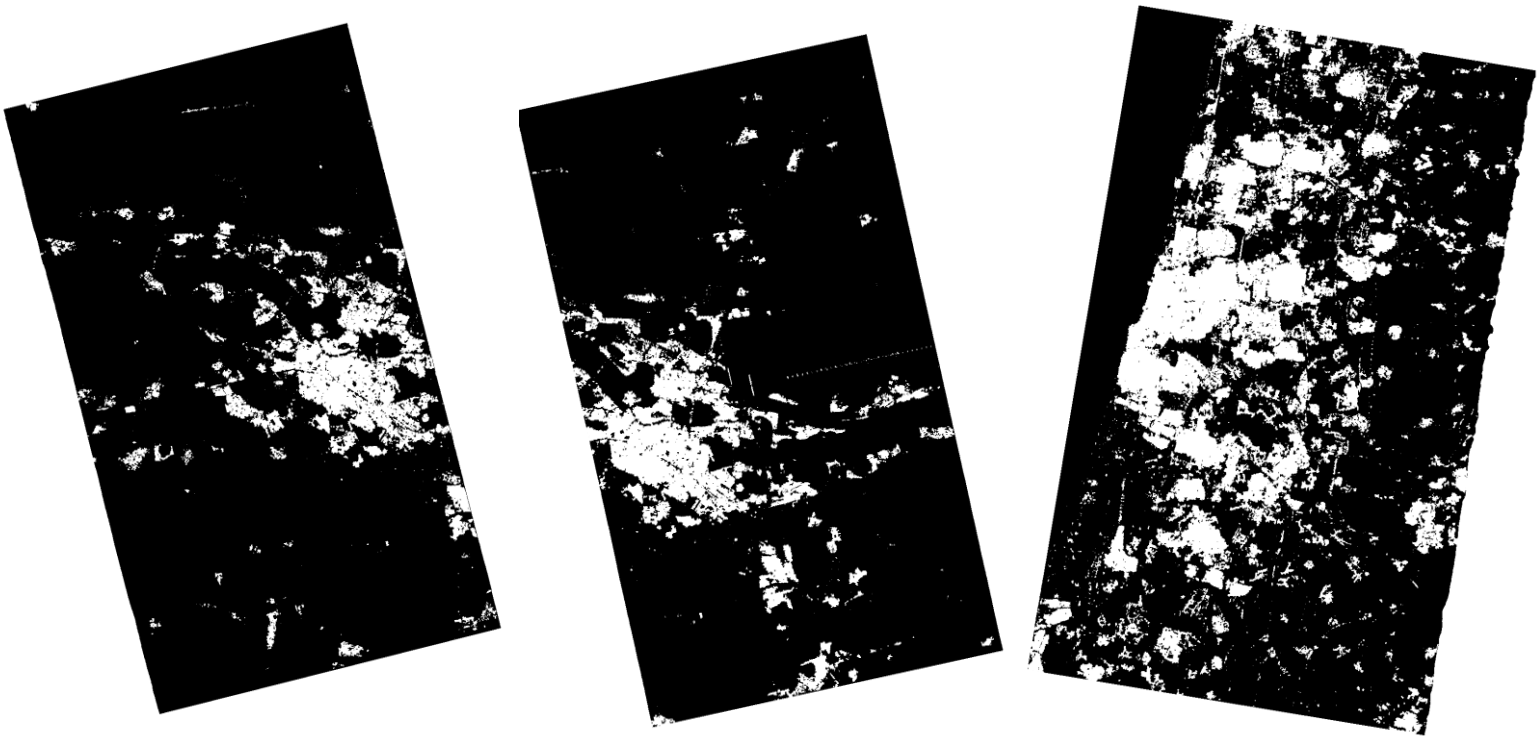

Figure 15 Urban footprint classification of Tjumen (left) and Tel Aviv (right) derived from TSX data.

In addition to the approach presented above based on VHR SAR data, also another method has been considered for retrieving the urban footprint from VHR optical images. In particular, RapidEye data have been taken into consideration. The RapidEye space segment consists of a constellation of five identical sun-synchronous EO satellites, which allow a global revisit time of only one day.

The approach applied on RapidEye data consists of an object-based procedure with two modules: segmentation and classification.

The basic task of the segmentation is to merge homogenous pixels into single segments in order to differentiate between heterogeneous neighboring regions (Benz et al. 2004). To this purpose, a bottom-up region-growing technique has been employed and homogeneous areas (e.g., water, grasslands) result in segments with a completely different shape with respect to those obtained over spectrally heterogeneous areas such as built-up areas.

In the classification phase the band ratio 'normalized difference vegetation index' (NDVI) is first used to mask natural environment areas. Then, for each segment different features (i.e., size, shape and spectral information) are extracted and provided as input to a fuzzy classifier, which provides as output a probability of class membership. If such probability is higher than a certain threshold, then the object is categorized as belonging to the urban class.

The resulting urban footprint for the city of Tel Aviv, Israel is provided in Figure 16. A visual assessment based on 150 randomly distributed samples resulted in an overall accuracy of 84.6%.

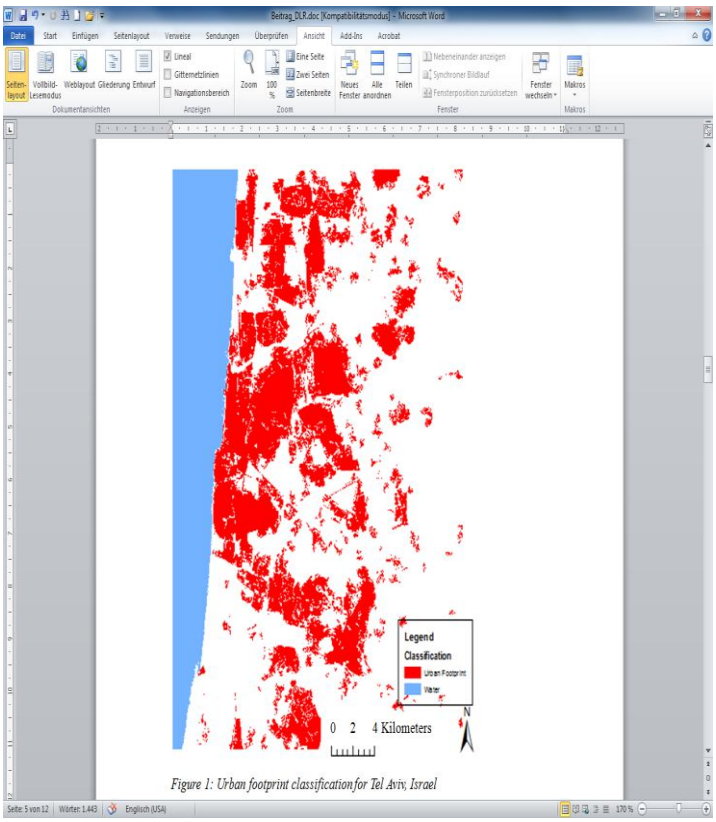

Figure 16. Urban footprint classification for Tel Aviv, Israel derived from RapidEye data.

It is worth noting that the urban footprint classification presented above can be further thematically refined by taking into consideration the percentage of impervious surfaces (PIS), which describes the entirety of impermeable surfaces including roads, buildings, parking lots, railroads or other infrastructural elements of urban areas such as squares and sidewalks. An effective technique for estimating PIS is that introduced by

Esch et al. 2009, which exploits Support Vector Regression. An example is provided in Figure 17, which reports the PIS computed for a Rapid Eye image acquired on 16th July 2012 over Tyumen.

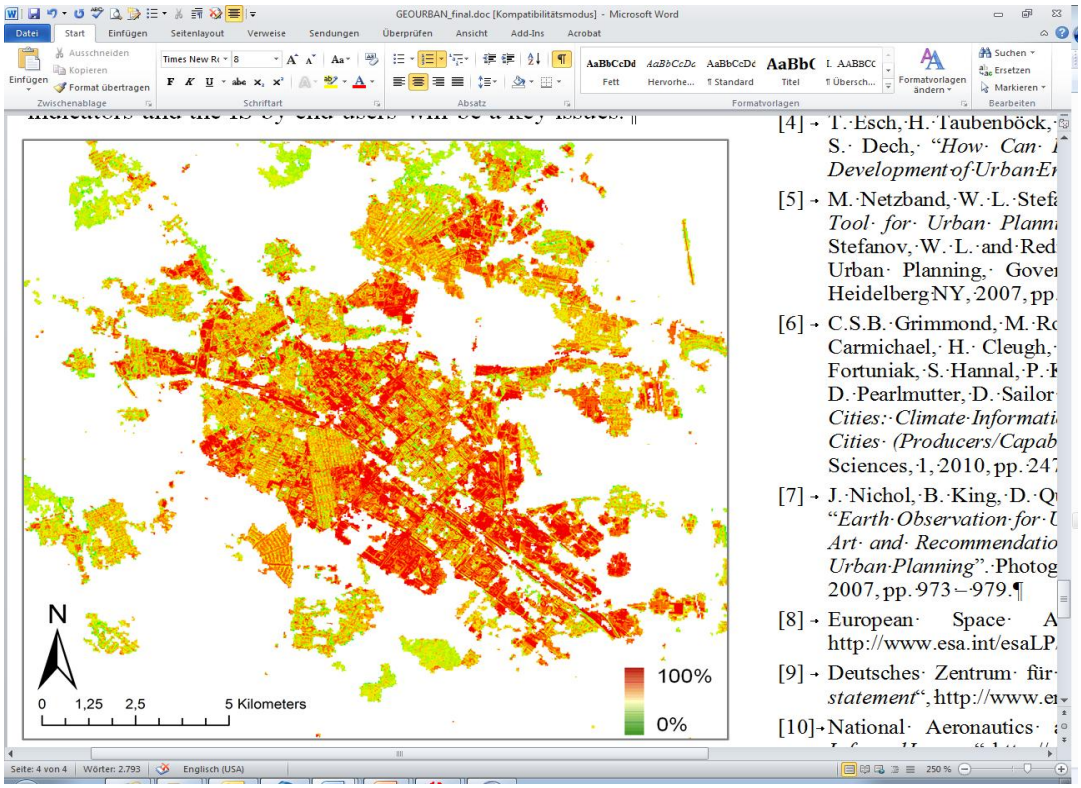

Figure 17. Percent impervious surface in the Tyumen region (RU), derived by combined analysis of RapidEye and TerraSAR-X data.